Supporting Information

Exploring Antiaromaticity in Single-Molecule Junctions formed from Biphenylene Derivatives

Markus Gantenbein[+1], Xiaohui Li[+2], Sara Sangtarash[+*3], Jie Bai[2], Gunnar Olsen[1], Afaf Alqorashi[3], Wenjing Hong[*2], Colin J. Lambert[*3], Martin R. Bryce[*1]

[1] Department of Chemistry, Durham University, DH1 3LE, Durham, UK

[2] State Key Laboratory of Physical Chemistry of Solid Surfaces, NEL, iChEM, College of Chemistry and Chemical Engineering, Xiamen University, Xiamen 361005, China

[3] Department of Physics, Lancaster University, LA1 4YB, Lancaster, UK

Emails of corresponding authors: s.sangtarash@lancaster.ac.uk; whong@xmu.edu.cn; c.lambert@lancaster.ac.uk; m.r.bryce@durham.ac.uk.

Table of Contents

1. Conductance Measurements

The mechanically controlled break junction (MCBJ) technique was used to characterize the conductance features of single-molecule junctions at ambient conditions, as shown in Figure S1. A laboratory-built bipotentiostat with a logarithmic current-voltage converter was used to record the raw data.[1,2]
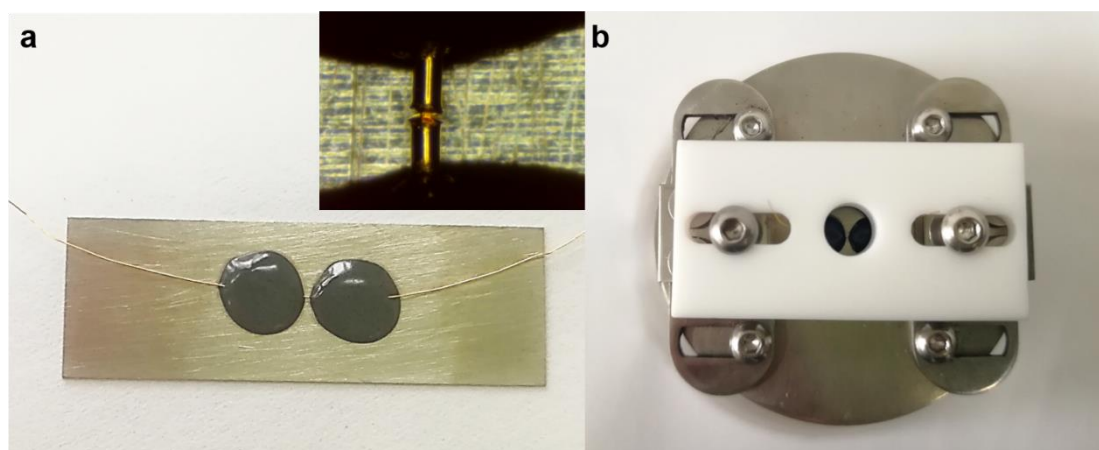
Figure S1. (a) Top-view of notched gold wire chip used in experiments. (b) Top-view of the mechanically controlled break junction (MCBJ) technique.

Before making the measurements a notched gold wire chip was prepared as follows: gold wire of 0.1 mm diameter (about 40 cm, 99.99%, Jiaming, Beijing) was fixed to a spring sheet (30 mm × 10 mm × 0.15 mm) with two drops of epoxy (mixture of Stycast 2850 FT and 3.5% catalyst 9) with polymerization for 6 h at 60 °C. Then the suspended part was partially excised to fabricate a constriction point as shown in the inset of Figure S1a. Next, the chip, polytetrafluoroethylene (PTFE) liquid cell and Kalrez O-ring were mounted on the MCBJ set-up. During the measurements, the breaking and connecting process of the notched gold-

wire was performed by the control of a combination of a stepping motor (Zaber NA14B16) and a piezo stack (Thorlab AE0505D18F). Simultaneously, the evolution of conductance characteristics during the breaking process was recorded for further statistical analysis.
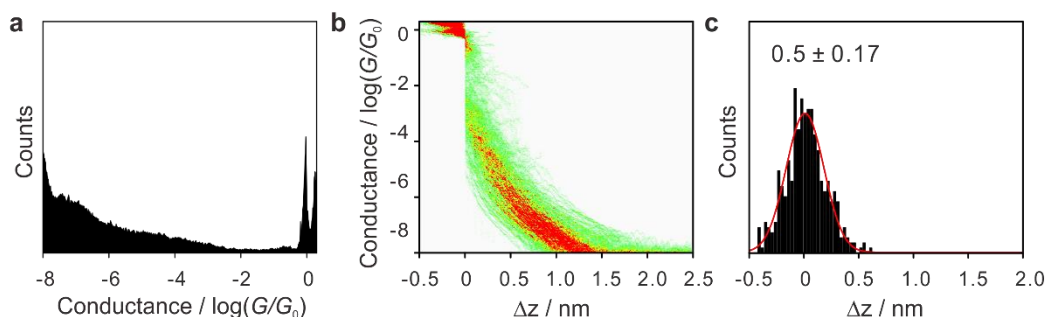
Figure S2. (a) One-dimensional (1D) conductance histogram measured in pure solvent (tetrahydrofuran:1,3,5-trimethylbenzene = 1:4, v/v) without a molecular junction peak. (b) Two-dimensional (2D) conductance-distance cloud with clear background. (c) The relative stretching distance histogram ranging from $10^{-0.3}$ to $10^{-6.0}$ G_0.
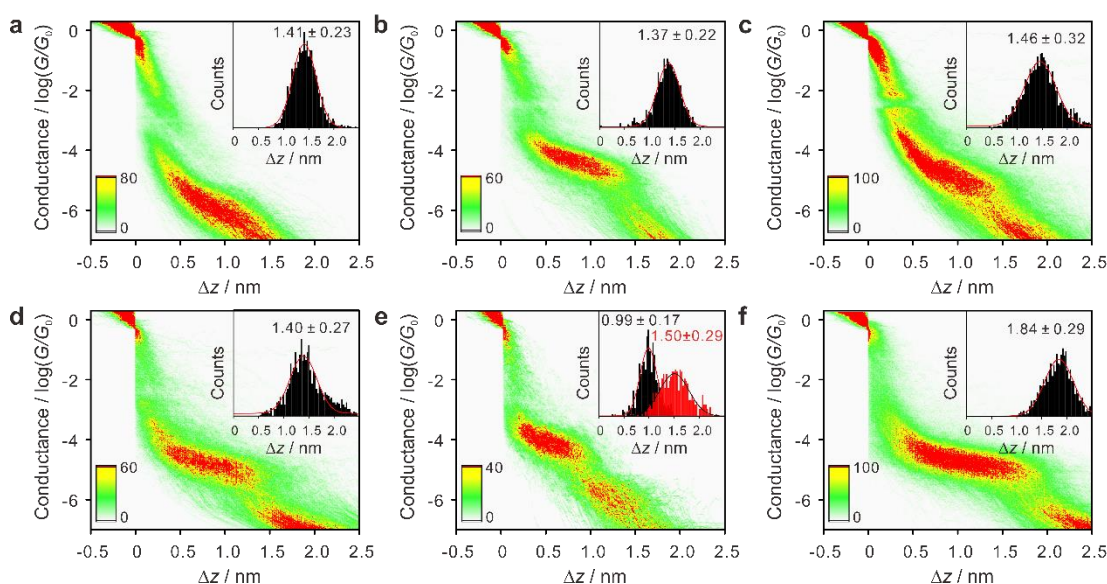
Figure S3. 2D conductance-distance clouds and the relative stretching distance histograms (insets) of **2** (a, inset ranging from $10^{-0.3}$ to $10^{-6.7}$ G_0), **3** (b, inset ranging from $10^{-0.3}$ to $10^{-5.4}$ G_0), **4** (c, inset ranging from $10^{-0.3}$ to $10^{-5.9}$ G_0), **6** (d, inset ranging from $10^{-0.3}$ to $10^{-5.8}$ G_0), **7** (e, black inset for high conductance state ranging from $10^{-0.3}$ to $10^{-5.1}$ G_0 and red inset for low conductance state ranging from $10^{-0.3}$ to $10^{-6.7}$ G_0), **8** (f, inset ranging from $10^{-0.3}$ to $10^{-5.7}$ G_0).

2. Theoretical Calculations

Both theoretical calculations and experimental measurements[3] show that cyclobutadiene has a rectangular geometry in the ground state with alternating carbon-carbon bond lengths of 1.34

Å and 1.58 Å as shown in Figure S4 (left). This longer bond length is comparable with the value found in biphenylene, where the two 6-membered rings were measured by X-ray crystallography to be 1.51-1.52 Å apart.[4] According to analysis of NMR data, the aromaticity of biphenylene relative to benzene is about 55% based on the relative bond fixing ability of the two aromatic systems.[5] As shown in Figure S4 (right), when located between two phenyl rings, the horizontal bonds of the four-membered ring are shortened and the vertical bonds are lengthened reflecting the fact that the fused phenyl rings lead to reduced antiaromaticity of the four-membered ring, compared with unsubstituted cyclobutadiene. On the other hand, the bond lengths of the 6-membered rings are no longer equal, which reflects the fact that the aromaticity of phenylene rings is reduced when they are connected via a four-membered ring in biphenylene.
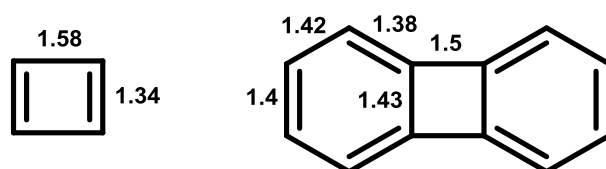
Figure S4: DFT calculated bond lengths (in Å) of cyclobutadiene and biphenylene.

To elucidate the effect of the two different bond lengths on the electronic properties of cyclobutadiene, rows (a) of Table S1 show the isosurfaces and energies of frontier orbitals, obtained from the unrelaxed structure, in which all four bond lengths are set equal to 1.44 Å. For comparison, rows (b) of Tables S1 show the orbital and energies of the relaxed structure of Figure S4 (left), in which the horizontal and vertical bonds are unequal. Clearly the main effect of the bond alternation is to remove the HOMO degeneracy of the unrelaxed structure. Since the bond lengths of the four-membered ring within biphenylene differ from those of the relaxed cyclobutadiene, rows (c) of Tables S1 show the isosurfaces and energies of frontier orbitals , obtained from an 'artificial' cyclobutadiene, in which the horizontal and vertical bond lengths are constrained to equal those shown in Figure S4 (right); i.e., 1.5 Å and 1.43 Å, respectively. Clearly this change in bond length compared with the relaxed cyclobutadiene produces only a qualitative change in the electronic structure, which barely affects the isosurfaces and produces minor shifts in the molecular energy levels. Finally, rows (d) of Tables S1 show the isosurfaces and energies of the frontier orbitals of biphenylene. As indicated by the circles in Table S1, in the region of the four-membered ring, the HOMO and

LUMO of biphenylene have the same symmetry as the HOMO and LUMO of cyclobutadiene.

Table S1: Eigenvalues and HOMO-LUMO orbitals of the 4-membered ring a) non-relaxed structure (square), b) relaxed structure c) structure relaxed between two 6-membered rings d) biphenylene

	E_F	HOMO-2	HOMO-1	HOMO	HOMO	HOMO	LUMO	LUMO+1	LUMO+2
a	-3.086	-8.223	-8.223	-7.508	-3.086	-3.086	0.96	3.514	3.514
b	-3.234	-8.061	-7.141	-3.862			-1.925	1.905	2.687
c	-2.975	-8.031	-7.279	-3.198			-2.752	1.697	3.057
d	-2.56	-6.223	-5.613	-4.42			-1.685	-1.18	0.377

It is interesting to apply the orbital product rule[6] to the HOMOs and LUMOs of these molecules. To apply the rule, the numbering system in Table S2 (left) is assigned to the pz orbitals of the biphenylene core. For molecules **1** and **3**, electrons are injected into and collected from the core via pz orbitals 1 and 4, whereas for molecules **2** and **4**, electrons are injected and collected via pz orbitals 2 and 7. Also note that in Table S1, regions of blue isosurfaces correspond to positive wavefunction amplitudes, whereas red regions correspond to negative wavefunction amplitudes. As indicated by the black arrows in Table S2, the HOMO is coloured red at both the injection and collection points, and therefore the product of the HOMO amplitudes at these points is positive. In contrast, as indicated by the green arrows, the LUMO amplitude at the injection point 1 is red, whereas the LUMO amplitude at

the collection point 4 is blue. Consequently the product of the LUMO amplitudes at these points is negative. The orbital product rule states that if the HOMO and LUMO products have opposite signs, then they interfere constructively, whereas if they have the same sign, they interfere destructively. Hence for molecules **1** and **3**, where electrons are injected into and collected from the core via pz orbitals 1 and 4, constructive quantum interference (CQI) is expected. Similarly for molecules **2** and **4**, where electrons are injected and collected via pz orbitals 2 and 7, CQI is expected, because the HOMO product is negative, whereas the LUMO product is positive. (i.e. the HOMO and LUMO products have opposite signs).

As an example of destructive quantum interference (DQI), consider the case of injection and collection via sites 3 and 7 Since the HOMO is coloured blue on site 3, but red on site 7, the HOMO product is negative. Similarly the LUMO product is positive on site 3 and negative on site 7, so the LUMO product is negative. Since both the HOMO and LUMO products have the same sign, they interfere destructively. In this latter example, the labels (3 and 7) assigned to the injection and collection sites are both odd. Inspection of the orbitals in Table S2 shows that if the injection and collection sites are either both even or both odd, then the HOMO and LUMO products have the same sign and exhibit DQI. On the other hand, if one of the injection and collection sites has an odd label and the other an even label, then the HOMO and LUMO products have opposite signs and exhibit CQI.

Table S2: Column 1: The numbering system used for the pz orbitals of biphenylene. This is the same as the standard International Union of Pure and Applied Chemistry (IUPAC) numbering of the carbon atoms of biphenylene. Columns 2 and 3: the HOMO and LUMO of biphenylene.
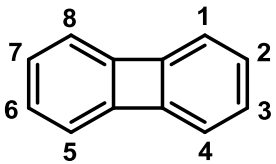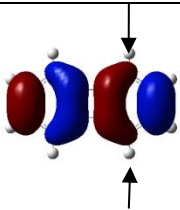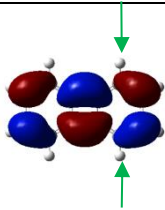
Demonstration that aromaticity or antiaromaticity could either increase or decrease the conductance depending on connectivity.

The fact that DQI occurs for odd-odd and even-even connectivities (i.e. when the injection and collection sites are either both odd or both even) is a consequence of the bipartite nature of the lattice shown in Table S2, where odd-numbered sites are connected to even-numbered sites only and vice versa. To illustrate this behaviour and to address the question of whether or not antiaromaticity is expected to increase or decrease electrical conductance, consider a simple tight binding model of biphenylene, in which each pz orbital is assigned a site energy ϵ_0 and each bond, except the horizontal bonds of the four-membered ring is assigned a value $-\gamma$. In what follows, ϵ_0 is chosen as the zero of energy and γ is chosen as the unit of energy, which is equivalent to choosing $\epsilon_0 = 0$ and $\gamma = 1$. With these choices, to examine the role of aromaticity, we consider the effect of varying the strength of the horizontal bonds labelled e in Figure S5, (which we denote $-\gamma_e$), while setting all other bonds γ to unity. Since bond strengths decrease with increasing bond length, values of γ_e less than unity model the effect of increasing the lengths of the horizontal bonds in the central four membered ring of biphenylene. In other words, $\gamma_e = 1$ corresponds to maximum aromaticity, whereas as γ_e decreases to values less than 1, the molecule becomes increasingly antiaromatic.
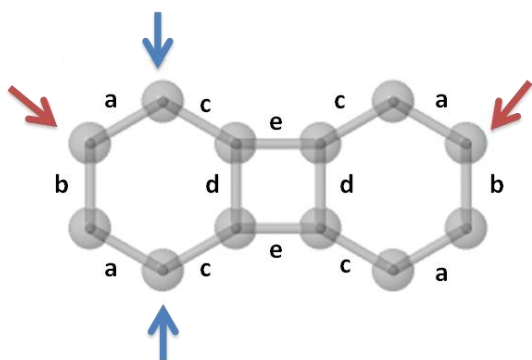
Figure S5. Labelling of bonds in a tight binding model of biphenylene.

Figure S6 shows the effect of increasing aromaticity on the transmission coefficient $T(E)$ of the biphenylene core with different connectivities. In each sub-plot, the legend shows the values of the horizontal bonds $-\gamma_e$ which vary from -1 (fully aromatic) to -0.2 (extensively antiaromatic). The labels such as 1-2, 1-3 etc. at the top of each sub-plot indicate the connectivity to the biphenylene core (i.e. the injection and collection sites). These results illustrate a number of interesting features:

1. As expected, for the even-even or odd-odd connectivities 1-3, 1-5, 1-7, 2-6, 2-8, the transmission coefficient at the middle of the HOMO-LUMO gap (i.e. at $E = 0$) vanishes, reflecting the fact that these connectivities exhibit DQI.

2.   For connectivities in which the injection site belongs to the left phenyl ring and the collection site belongs to the right phenyl ring, such as 1-5, 1-6, 1-7, 1-8, 2-5, 2-6, 2-7, anti-aromaticity (i.e. decreasing γ_e) decreases the transmission within the gap and hence decreases the electrical conductance. One exception is the connectivity 1-5, which increases initially, because the anti-resonance at $\gamma_e = 1$ is formed from additional satellite anti-resonances, which merge at $\gamma_e = 1$.

3.   When the injection and collection sites belong to the same phenyl ring, antiaromaticity can either increase the transmission within the gap (as for the *ortho* and *para* connectivities 1-2 and 1-4) or decrease the transmission within the gap (as for the *meta* connectivity 1-3 and *ortho* connectivity 2-3).

Based on these results, we conclude that aromaticity or antiaromaticity can either increase or decrease the π–system contribution to electrical conductance, depending on connectivity.
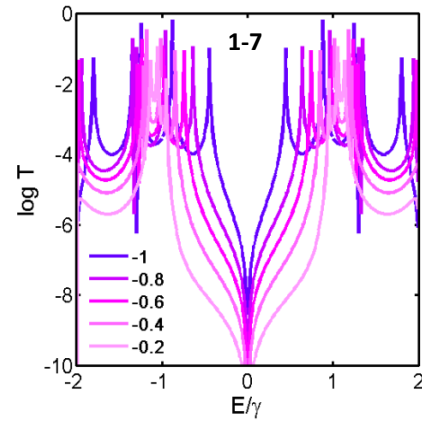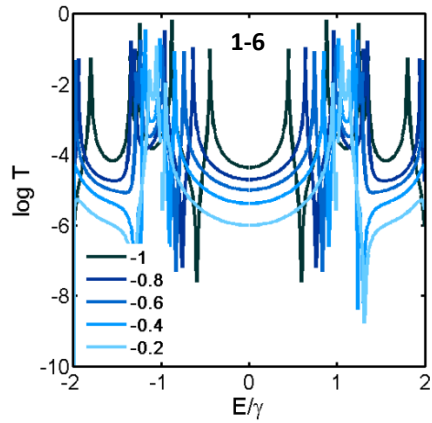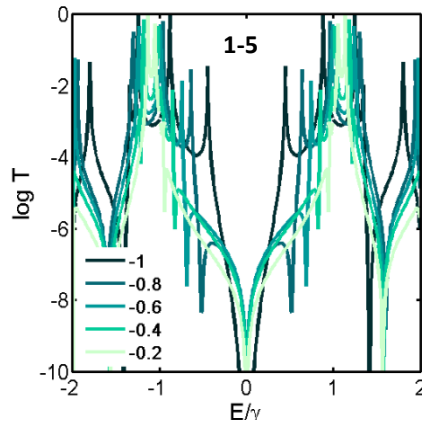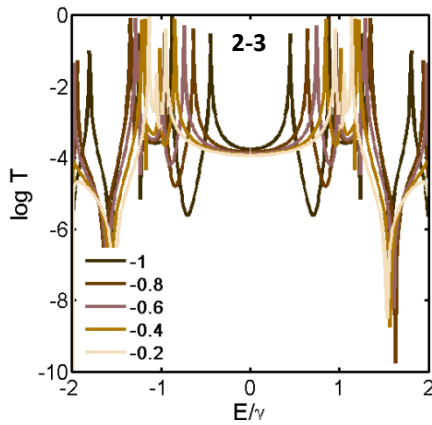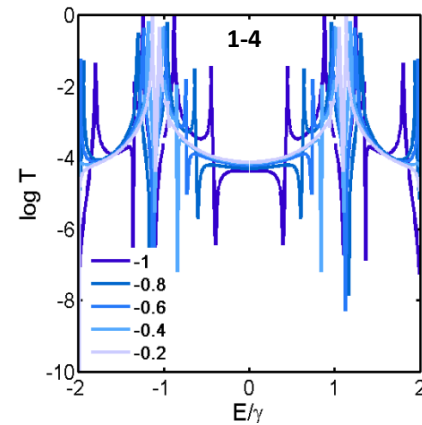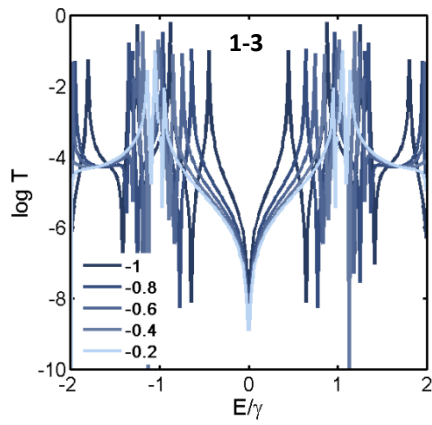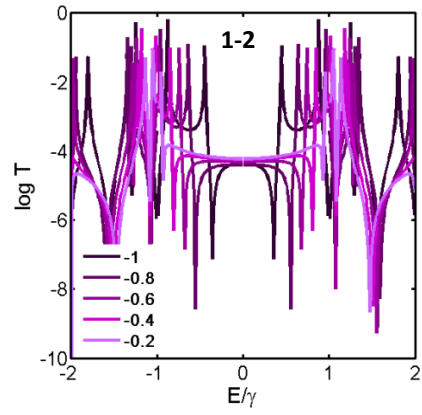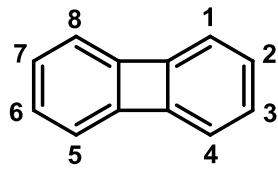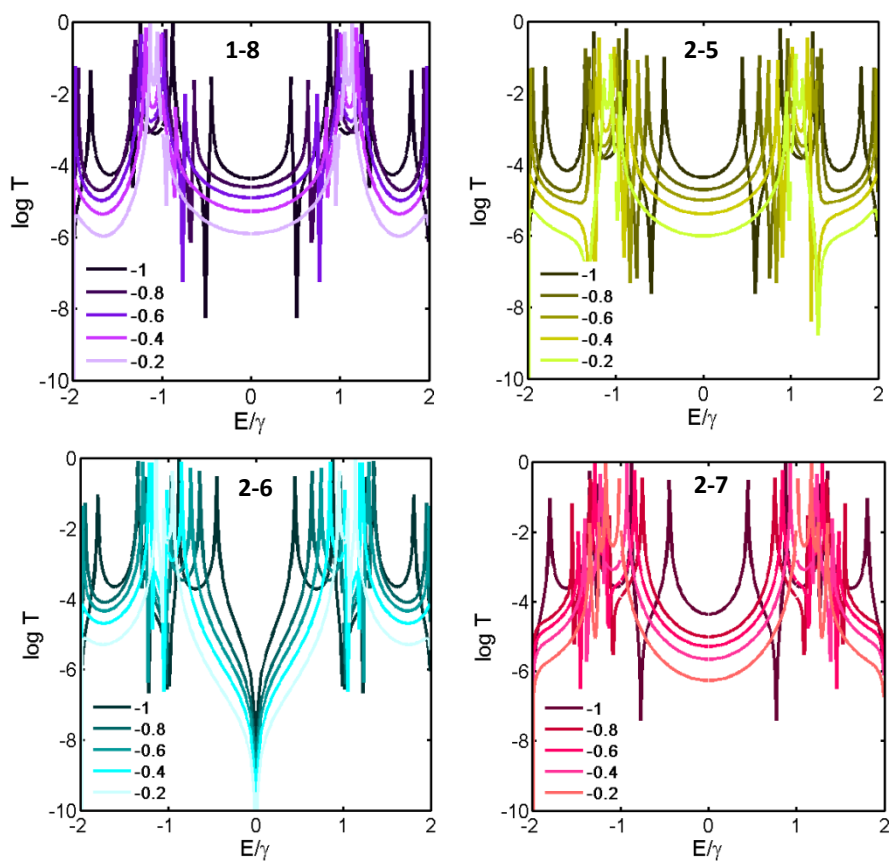
Figure S6: Structure of the system and corresponding tight binding transmission coefficient of the molecule with different connectivities based on the numbering system used for the pz orbitals of biphenylene. In all figures the dark color represents the matrix with ε_0=o and γ=-1. This corresponds to the choices $\gamma_e = -0.8, -0.6, -0.4, -0.2$ as shown in the legend.

Clearly in the limit $\gamma_e = 0$, the two phenyl rings are decoupled and therefore the energy level spectrum corresponds to that of two isolated rings. Figure S7 shows how the energy levels of this tight binding model depend on γ_e.
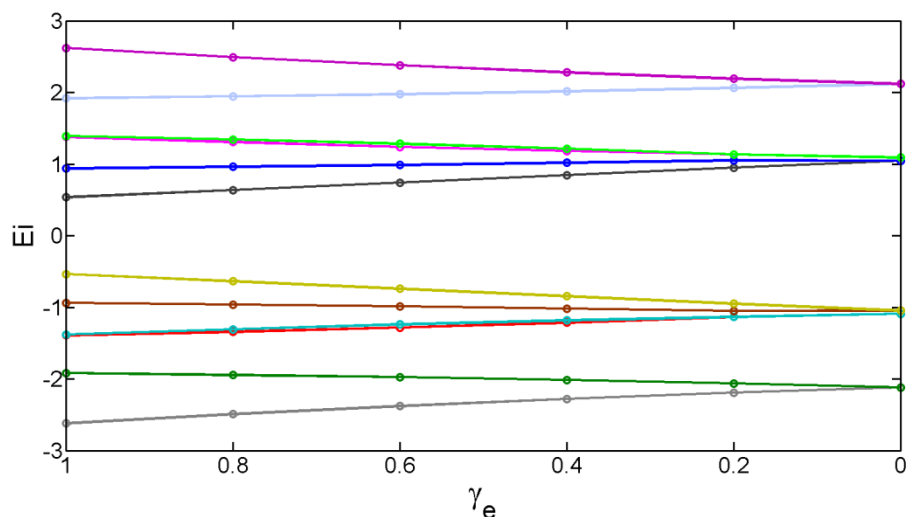
Figure S7: Eigenvalues (Ei) of structures in Figure S6 for different values of the coupling γ_e.

Figure S8 shows that with an appropriate choice of γ_e, the tight binding models of molecules **3**, **5** and **7** are in good agreement with the experimental trends.
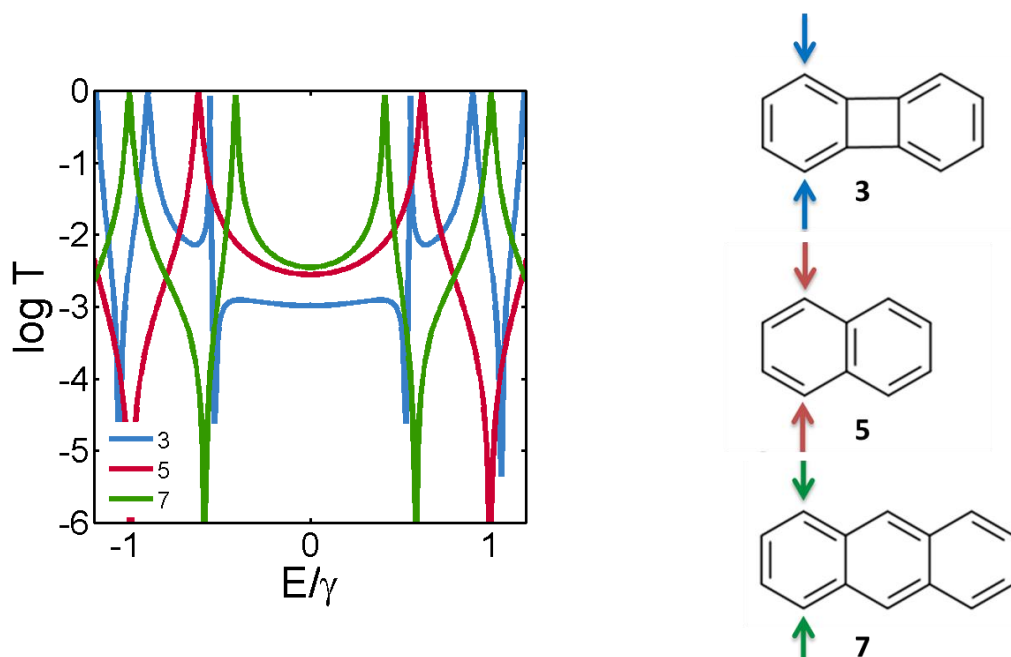
Figure S8: a) Tight binding transmission coefficients of molecules **3**, **5** and **7**, where all $\varepsilon_0=0$ and $\gamma = -1$, except $\gamma_e = -0.8$ for molecule **3**.

Computational Methods

The optimized geometry and ground state Hamiltonian and overlap matrix elements of each structure were self-consistently obtained using the SIESTA[7] implementation of density functional theory (DFT). SIESTA employs norm-conserving pseudo-potentials to account for

the core electrons and linear combinations of atomic orbitals to construct the valence states. The generalized gradient approximation (GGA) of the exchange and correlation functional is used with the Perdew-Burke-Ernzerhof parameterization (PBE), a double-ζ polarized (DZP) basis set, a real-space grid defined with an equivalent energy cut-off of 250 Ry. The geometry optimization for each structure is performed to the forces smaller than 10 meV/Å. Figure S9 shows geometry-optimized structures used to obtain the DFT results in Figure 3 of the manuscript. The mean-field Hamiltonian obtained from the converged DFT calculation or a simple tight-binding Hamiltonian was combined with the Gollum quantum transport code[8] to calculate the phase-coherent, elastic scattering properties of each system consisting of left (source) and right (drain) leads and the scattering region. The transmission coefficient $T(E)$ for electrons of energy E (passing from the source to the drain) is calculated via the relation $T(E) = Trace(\Gamma_R(E)G^R(E)\Gamma_L(E)G^{R\dagger}(E))$. In this expression, $\Gamma_{L,R}(E) = i\left(\sum_{L,R}(E) - \sum_{L,R}{}^{\dagger}(E)\right)$ describe the level broadening due to the coupling between left (L) and right (R) electrodes and the central scattering region, $\sum_{L,R}(E)$ are the retarded self-energies associated with this coupling, and $G^R = (ES - H - \sum_L - \sum_R)^{-1}$ is the retarded Green's function, where H is the Hamiltonian and S is overlap matrix. Using the obtained transmission coefficient ($T(E)$), the conductance could be calculated by the Landauer formula ($G = G_0 \int dE\ T(E)(-\partial f/\partial E)$) where $G_0 = 2e^2/h$ is the conductance quantum, $f(E) = (1 + exp((E - E_F)/k_B T))^{-1}$ is the Fermi-Dirac distribution function, T is the temperature and $k_B = 8.6 \times 10^{-5}$ eV/K is the Boltzmann's constant.
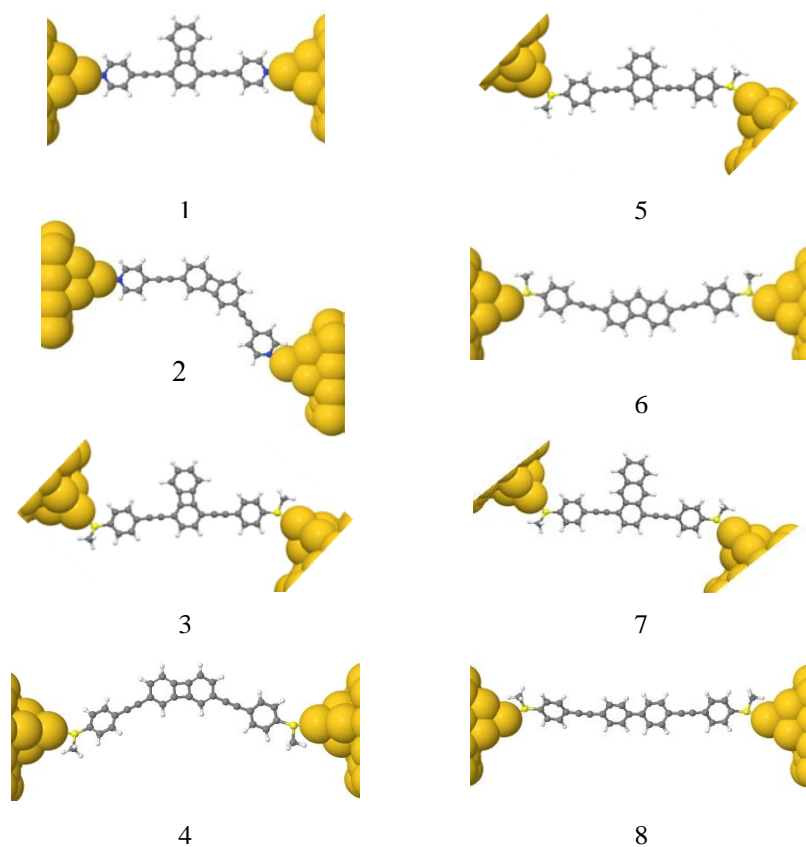
Figure S9: Relaxed structures of molecules **1-8.**

Frontier Orbitals

Table S3: Frontier orbitals and energies of molecules **1-8**. Units are eV; for the orbitals red = negative amplitude, blue = positive.

	HOMO-2	HOMO-1	HOMO	LUMO	LUMO+1	LUMO+2
	-7.0477	-6.394	-6.0953	-2.5306	-2.0898	-1.4585
1						
	-6.9933	-6.8844	-5.8776	-2.6122	-1.8231	-1.6054
2						
	-6.1497	-5.6871	-5.5511	-1.9864	-1.7143	-0.8435
3						
	-6.258	-5.8504	-5.3334	-2.1605	-1.2435	-1.2408
4						
	-6.4218	-6.0137	-5.3606	-2.1633	-0.9061	-0.6993
5						
	-6.4218	-5.8232	-5.3878	-1.9265	-1.1619	-0.6830
6						
	-6.0409	-6.0137	-5.2245	-2.3837	-1.2707	-0.9170
7						
	-6.5307	-5.8232	-5.5239	-1.9047	-1.2517	-0.5197
8						

Table S3 shows that the amplitude of the HOMO of **1** is the same colour (red) at both ends of the molecule and therefore the product of these amplitudes is positive. Similarly the amplitude of the LUMO of **1** is the same colour (blue) at both ends of the molecule and therefore the product of these amplitudes is also positive. The orbital product rule[6] tells us that when the HOMO product of a molecule has the same sign as the LUMO product, destructive quantum interference (DQI) is expected within the HOMO-LUMO gap, signalled by a sharp dip in the transmission function. On the other hand, when the products have opposite signs, constructive quantum interference (CQI) is expected. Therefore, DQI is expected within the HOMO-LUMO gap of **1**. The associated transmission dip is located at $E - E_F^{DFT} = -1.8\ eV$ in Figure 3a of the manuscript. In all other cases, the HOMO and LUMO products have opposite signs and therefore no DQI feature is expected within the HOMO-LUMO gap, in agreement with Figure 3 of the manuscript. On the other hand, with the exception of **7**, the HOMO-1 of the each molecule has an opposite sign to the HOMO and therefore there should be no DQI features between the HOMO-1 and the HOMO of each

molecule, except for **7**. In the case of **7**, this DQI transmission dip is located at $E - E_F^{DFT} = -1.8\ eV$ in Figure 3a of the manuscript.

3. Synthesis and Characterization of Molecules

a.　　General Information

All reactions were carried out under an argon atmosphere unless otherwise stated. Starting materials were purchased commercially and were used as received. Solvents were dried using an Innovative Technology solvent purification system and were stored in ampoules under argon. Analytical thin layer chromatography (TLC) was performed on 20 mm pre-coated plates of silica gel (Merck, silica gel 60 F_{254}) TLC plates and spots were visualised using a TLC lamp emitting at 365, 312 or 254 nm. Silica gel column chromatography was performed using silica gel 60 purchased from Sigma Aldrich or Fluorochem. UV–Visible absorption spectra were recorded at room temperature on a Thermo Scientific Evolution 220 spectrometer. ^{1}H and ^{13}C NMR spectroscopy was carried out on Bruker AV400, Varian VNMRS 500 and 700, and Varian Inova 500 NMR spectrometers. Chemical shifts are reported in ppm relative to $CHCl_3$ (7.26 ppm), and all NMR data was processed in MestReNova V10. Melting points were carried out on a Stuart SMP40 machine using open ended capillaries with a ramping rate of 1 °C min^{-1}. Videos were replayed manually to determine the melting point. High resolution mass spectroscopy was carried out on a Waters LCT Premier XE using ASAP ionization. Samples were analysed directly as solids. Elemental analysis was performed on an Exeter Analytical E-440 machine.

b.　　Experimental Procedures

Synthesis of compounds 1 and 3

The synthetic scheme is shown in Scheme 1 of the manuscript.

1-Bromo-4,5-dichloro-2-iodobenzene (**10)** was synthesised from **9** according to a literature procedure. Its ^{1}H- and ^{13}C-NMR spectra matched the previously reported data.[9]

2,2'-dibromo-4,5-dichloro-1,1'-biphenyl (11)
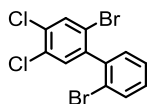
A solution of 1-bromo-4,5-dichloro-2-iodobenzene (**10**) (1.20 g, 3.4 mmol), (2-bromophenyl) boronic acid (0.80 g, 4.1 mmol), toluene (15 mL), and ethanol (8 mL) was degassed for 30 min. Afterwards, a degassed solution of aqueous Na_2CO_3 (1 M, 8 mL) and $Pd(PPh_3)_4$ (197.1 mg, 5% mmol) was added and the resulting reaction mixture was stirred at 110 °C for 15 h under inert atmosphere. The reaction was then filtered through a pad of Celite[TM], and solvents were removed under reduced pressure. The residue was diluted in petroleum ether, washed sequentially with saturated aqueous NH_4Cl, water and brine. The organic layer was separated and dried over $MgSO_4$ and removed *in vacuo*. The crude product was further purified by flash column chromatography (SiO_2, petroleum ether) yielding **11** (1.10 g, 2.9 mmol, 85%) as a colourless oil. ^{1}H NMR (400 MHz, Acetone-d_6, δ): 7.98 (s, 1H), 7.75 (dd, J = 7.9, 1.2 Hz, 1H), 7.55 (s, 1H), 7.52 (td, J = 7.5, 1.2 Hz, 1H), 7.41 (td, J = 7.9, 1.8 Hz, 1H), 7.36 (dd, J = 7.5, 1.8 Hz, 1H). ^{13}C NMR (101 MHz, Acetone-d_6, δ): 143.46, 140.95, 134.70, 133.68, 133.45, 133.29, 132.18, 132.04, 131.50, 128.79, 123.75, 123.11. HRMS–ASAP+ (m/z): calcd for $C_{12}H_6Br_2Cl_2$ $[M]^{\bullet+}$, 377.8213; found, 377.8231.

2,3-dichlorobiphenylene (12)
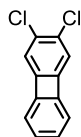
An oven-dried argon-flushed flask was charged with 2,2'-dibromo-4,5-dichloro-1,1'-biphenyl (**11**) (2.50 g, 6.6 mmol), dry THF (80 mL), and cooled to –78 °C. Afterwards, *n*-BuLi (2.5 M in hexanes, 6.0 mL, 15.1 mmol) was added dropwise and the resulting reaction mixture was stirred for 1 h at –78 °C under inert atmosphere. Meanwhile, a separate oven-dried argon-flushed flask was charged with $ZnCl_2$ (0.7 M in THF, 12.2 mL, 8.5 mmol) and dry THF (40 mL) and this solution was transferred via cannula into the reaction mixture at –50 °C. After stirring at this temperature, the reaction mixture was cooled to –78 °C and $CuCl_2$ (2.6 g, 19.7 mmol) was added in one portion. The resulting reaction mixture was allowed to warm to room temperature overnight. The reaction was then quenched by the addition of saturated aqueous NH_4Cl and diluted with petroleum ether. The organic layer was washed sequentially with saturated aqueous NH_4Cl, water and brine, dried over $MgSO_4$, and solvents were

removed at reduced pressure. The crude product was purified by flash column chromatography (SiO$_2$, petroleum ether) yielding **12** (851.0 mg, 3.8 mmol, 59%) as a yellow solid. ^{1}H NMR (400 MHz, Acetone-d$_6$, δ): 6.91 (dd, J = 5.0, 2.9 Hz, 2H), 6.88 (s, 2H), 6.84 (dd, J = 5.0, 2.9 Hz, 2H). ^{13}C NMR (101 MHz, Acetone-d$_6$, δ): 151.97, 149.96, 131.62, 130.69, 120.83, 119.84. HRMS–ASAP+ (m/z): calcd for C$_{12}$H$_6$Cl$_2$ [M]$^{\bullet+}$, 219.9847; found, 219.9846.

1,4-bis(trimethylsilane)-2,3-dichlorobiphenylene (13)
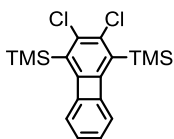
An oven-dried argon-flushed flask was charged with 2,3-dichlorobiphenylene (**12**) (0.70 g, 3.2 mmol) and dry THF (30 mL). Resulting reaction mixture was cooled at −78 °C, followed by the addition of TMSCl (0.80 g, 7.0 mmol) and freshly prepared lithium diisopropylamide solution (LDA, 135.0 mM in THF, 52 mL, 7.0 mmol). The resulting reaction mixture was allowed to warm to room temperature overnight. The reaction was then quenched by the addition of saturated aqueous NH$_4$Cl and diluted with diethyl ether. The organic layer was washed sequentially with saturated aqueous NH$_4$Cl, water and brine, dried over MgSO$_4$, and solvents were removed at reduced pressure. The crude product was purified by flash column chromatography (SiO$_2$, petroleum ether) affording **13** (1.00 g, 2.8 mmol, 89%) as a yellow solid. ^{1}H NMR (400 MHz, CDCl$_3$, δ): 6.85–6.78 (m, 4H), 0.39 (s, 18H). ^{13}C NMR (101 MHz, CDCl$_3$, δ): 156.90, 151.29, 137.16, 132.97, 128.92, 119.90, 0.73. HRMS–ASAP+ (m/z): calcd for C$_{18}$H$_{22}$Cl$_2$Si$_2$ [M]$^{\bullet+}$, 364.0637; found, 364.0648.

1,4-bis(trimethylsilyl)biphenylene (14)
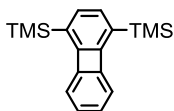
An oven-dried argon-flushed flask was charged with 1,4-bis(trimethylsilane)-2,3-dichlorobiphenylene (**13**) (570 mg, 1.6 mmol) and dry THF/Et$_2$O (15 mL, 1:1 v/v). The resulting reaction mixture was cooled at −78 °C, followed by the dropwise addition of *t*-BuLi (1.7 M in pentane, 4.6 mL, 7.8 mmol). After stirring at −78 °C for 1 h, the cooling bath was removed and reaction mixture was allowed to warm to room temperature, before the reaction

was quenched by the addition of saturated aqueous NH_4Cl and diluted with diethyl ether. The organic layer was washed sequentially with saturated aqueous NH_4Cl, water and brine, separated and dried over $MgSO_4$, and solvents were removed *in vacuo*. The crude product was purified by flash column chromatography (SiO_2, petroleum ether) yielding **14** (410 mg, 1.4 mmol, 88%) as a yellow oil. ^{1}H NMR (400 MHz, Acetone-d_6, δ): 6.84 (s, 2H), 6.78–6.70 (m, 4H), 0.26 (s, 18H). ^{13}C NMR (101 MHz, Acetone-d_6, δ): 157.77, 153.94, 132.83, 131.46, 129.29, 118.97, −1.37. HRMS–ASAP+ (m/z): calcd for $C_{18}H_{24}Si_2$ [M]$^{\bullet+}$, 296.1417; found, 296.1418.

1,4-diiodobiphenylene (15)
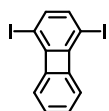
An oven dried argon flushed flask was charged with 1,4-bis(trimethylsilyl)biphenylene (**14**) (550 mg, 1.9 mmol) and dry methylene chloride (15 mL). The resulting reaction mixture was cooled to 0 °C, followed by the addition of ICl (1 M in methylene chloride, 4.1 mL, 4.1 mmol). After stirring at room temperature for 1 h, the reaction was quenched by the addition of saturated aqueous $Na_2S_2O_3$, followed by extraction with methylene chloride (3 x 50 mL). the combined organic layers were washed with brine, dried over $MgSO_4$, and the solvent was removed at reduced pressure. The crude product was purified by flash column chromatography (SiO_2, hexane/methylene chloride, 20:1 v/v) affording **15** (710 mg, 1.7 mmol, 95%) as a yellow solid. ^{1}H NMR (400 MHz, $CDCl_3$, δ): 6.98–6.84 (m, 4H), 6.66 (s, 2H). ^{13}C NMR (101 MHz, $CDCl_3$, δ): 158.05, 149.50, 137.76, 129.70, 117.05, 80.04. HRMS–ASAP+ (m/z): calcd for $C_{12}H_6I_2$ [M]$^{\bullet+}$, 403.8559; found, 403.8568.

1,4-bis(4-pyridylethynyl)biphenylene (1)
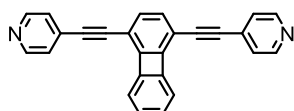
An oven-dried argon-flushed flask was charged with 1,4-diiodobiphenylene (**15**) (200.0 mg, 0.5 mmol), dry THF (10 mL), and dry diisopropylethylamine (DIPEA, 1 mL). The resulting mixture was degassed for 20 min followed by the sequential addition of Pd(dba)$_2$ (28.5 mg, 10 mol%), CuI (18.9 mg, 20 mol%), and PPh$_3$ (51.9 mg, 40 mol%). After further degassing

for 5 min, 4-ethynylpyridine (142.9 mg, 1.4 mmol) was added and the reaction was stirred at 35 °C for 4 h. After completion, the reaction was filtered through a pad of Celite^{TM}, and the residue was diluted in ethyl acetate, washed sequentially with saturated aqueous NH_4Cl, water and brine. The organic layer was dried over $MgSO_4$ and solvent was removed *in vacuo*. The crude product was purified by flash column chromatography (SiO_2, toluene/ethyl acetate, 5:1 (v/v), 5% triethylamine) affording **1** (132.0 mg, 0.4 mmol, 75%) as a yellow solid. ^1H NMR (400 MHz, $CDCl_3$, δ): 8.64–8.62 (m, 4H), 8.64–8.62 (m, 4H), 6.90–6.83 (m, 4H), 6.82 (s, 2H). ^{13}C NMR (101 MHz, $CDCl_3$, δ): 153.88, 150.04, 149.58, 131.05, 130.73, 129.92, 125.63, 118.82, 111.71, 90.73, 89.94. HRMS–ASAP+ (m/z): calcd for $C_{26}H_{15}N_2$ [M]+H, 355.1235; found, 355.1235.

1,4-bis(ethynyl-4-(methylsulfanyl)benzene)biphenylene (3)
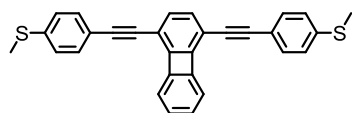
An oven-dried argon-flushed flask was charged with 1,4-diiodobiphenylene (70.0 mg, 0.2 mmol), dry THF (5 mL), and dry DIPEA (0.5 mL). The resulting mixture was degassed for 15 min followed by the sequential addition of $PdCl_2(PPh_3)_2$ (6.1 mg, 5 mol%), CuI (3.3 mg, 10 mol%), and PPh_3 (6.8 mg, 15 mol%). After further degassing for 5 min, 1-ethynyl-4-(methylsulfanyl)benzene (77.1 mg, 0.5 mmol) was added and the reaction was stirred at 35 °C for 2 h. After completion, the reaction was filtered through a pad of Celite^{TM}, and the residue was diluted in methylene chloride, washed sequentially with saturated aqueous NH_4Cl, water and brine. The organic layer was dried over $MgSO_4$ and removed at reduced pressure. The crude product was purified by flash column chromatography (SiO_2, hexane/methylene chloride, 10:1 (v/v)) affording **3** (67.0 mg, 0.15 mmol, 87%) as a yellow solid. ^1H NMR (400 MHz, Acetone-d_6, δ): 7.53–7.51 (m, 4H), 7.33–7.30 (m, 4H), 6.94–6.93 (m, 4H), 6.88 (s, 2H) 2.54 (s, 6H). ^{13}C NMR (101 MHz, $CDCl_3$, δ): 152.89, 149.98, 140.02, 132.06, 130.73, 129.32, 125.98, 119.30, 118.36, 112.29, 93.33, 85.98, 15.50. HRMS–ASAP+ (m/z): calcd for $C_{30}H_{21}S_2$ [M]+H, 445.1085; found, 445.1081.

Synthesis of compounds 2 and 4
The synthetic scheme is shown in Scheme 2 of the manuscript.

Compound **16** was synthesised according to the literature procedure. Its ^{1}H- and ^{13}C-NMR spectra matched previously reported data.[10]

2,7-dibromobiphenylene (17)
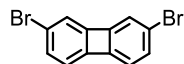
An oven-dried argon-flushed flask was charged with 4,4'-dibromo-2,2'-diiodo-1,1'-biphenyl (**16**) (2.40 g, 4.3 mmol), dry THF (50 mL), and cooled to −78 °C. Afterwards, *n*-BuLi (2.5 M in hexanes, 3.8 mL, 9.4 mmol) was added dropwise and the resulting reaction mixture was stirred for 1 h at −78 °C under inert atmosphere. Meanwhile, a separate oven-dried argon-flushed flask was charged with ZnCl$_2$ (0.7 M in THF, 6.7 mL, 4.7 mmol) and dry THF (25 mL) and this solution was transferred via cannula into the reaction mixture at −50 °C. After stirring at this temperature, the reaction mixture was cooled to −78 °C, and CuCl$_2$ (1.7 g, 12.8 mmol) was added in one portion. The resulting reaction mixture was allowed to warm to room temperature overnight. The reaction was then quenched by the addition of saturated aqueous NH$_4$Cl and diluted with petroleum ether. The organic layer was washed sequentially with saturated aqueous NH$_4$Cl, water and brine, dried over MgSO$_4$, and solvents were removed at reduced pressure. The crude product was further purified by flash column chromatography (SiO$_2$, petroleum ether) yielding **17** (802 mg, 2.6 mmol, 61%) as a yellow solid. ^{1}H NMR (400 MHz, CDCl$_3$, δ): 6.96 (dd, J = 7.3, 1.5 Hz, 2H), 6.78 (dd, J = 1.5, 0.7 Hz, 2H), 6.53 (dd, J = 7.3, 0.7 Hz, 2H). ^{13}C NMR (101 MHz, CDCl$_3$, δ): 151.14, 148.64, 131.30, 121.80, 119.12. HRMS–ASAP+ (m/z): calcd for C$_{12}$H$_6$Br$_2$ [M]$^{•+}$, 307.8836; found, 307.8842.

2,7-bis(4-pyridylethynyl)biphenylene (2)
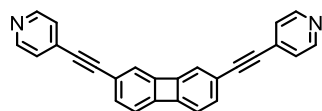
An oven-dried argon-flushed flask was charged with 2,7-dibromobiphenylene (**17**) (270.0 mg, 0.9 mmol), dry 1,4-dioxane (15 mL), and dry DIPEA (10 mL). The resulting mixture was degassed for 20 min followed by the sequential addition of PdCl$_2$(PhCN)$_2$ (33.4 mg, 10 mol%), CuI (33.2 mg, 20 mol%), and P(*t*-Bu)$_3$ (70.5 mg, 40 mol%). After further degassing for 5 min, 4-ethynylpyridine (251.5 mg, 2.4 mmol) was added and mixture was stirred at 85

°C for 16 h. The mixture was filtered through a pad of Celite[TM], and the residue was diluted in ethyl acetate, washed sequentially with saturated aqueous NH_4Cl, water and brine. The organic layer was dried over $MgSO_4$ and solvents were removed at reduced pressure. The crude product was purified by flash column chromatography (SiO_2, ethyl acetate/toluene, 2:1 (v/v), 5% triethylamine) affording **2** (218.0 mg, 0.6 mmol, 70%) as a yellow solid. ^{1}H NMR (400 MHz, $CDCl_3$, δ): 8.61–8.59 (m, 4H), 7.35–7.34 (m, 4H), 7.10 (dd, J = 7.2, 1.2 Hz, 2H), 6.86 (t, J = 1.1 Hz, 2H), 6.75 (dd, J = 7.2, 0.9 Hz, 2H). ^{13}C NMR (101 MHz, $CDCl_3$, δ): 151.23, 150.35, 149.96, 133.94, 131.41, 125.56, 122.54, 120.44, 118.17, 94.44, 87.43. HRMS–ASAP+ (m/z): calcd for $C_{26}H_{15}N_2$ [M]+H, 355.1235; found, 355.1232.

2,7-bis(ethynyl-4-(methylsulfanyl)benzene)biphenylene (4)
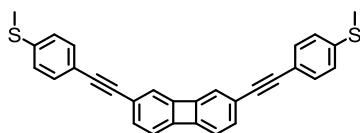
An oven-dried argon-flushed flask was charged with 2,7-dibromobiphenylene (**17**) (80.0 mg, 0.3 mmol), dry 1,4-dioxane (7 mL), and dry DIPEA (3 mL). The resulting mixture was degassed for 15 min followed by the sequential addition of $PdCl_2(MeCN)_2$ (6.7 mg, 10 mol%), CuI (9.8 mg, 20 mol%), and P(*t*-Bu)$_3$ (20.1 mg, 40 mol%). After further degassing for 5 min, 1-ethynyl-4-(methylsulfanyl)benzene (95.6 mg, 0.6 mmol) was added and reaction was stirred at 85 °C for 16 h. The reaction was filtered through a pad of Celite[TM], and the residue was diluted in ethyl acetate, washed sequentially with saturated aqueous NH_4Cl, water and brine. The organic layer was dried over $MgSO_4$ and solvents were removed at reduced pressure. The crude product was purified by flash column chromatography (SiO_2, hexane/methylene chloride, 10:1 (v/v)) affording **4** (56 mg, 0.1 mmol, 49%) as a yellow solid. ^{1}H NMR (400 MHz, $CDCl_3$, δ): 7.41–7.39 (m, 4H), 7.21–7.19 (m, 4H), 7.01 (dd, J = 7.2, 1.2 Hz, 2H), 6.80 (t, J = 1.1 Hz, 2H), 6.66 (dd, J = 7.2, 0.9 Hz, 2H), 2.50 (s, 6H). ^{13}C NMR (101 MHz, $CDCl_3$, δ): 150.37, 150.34, 139.53, 132.96, 131.96, 126.05, 123.50, 120.25, 119.63, 117.83, 90.24, 89.92, 15.55. HRMS–ESI– (m/z): calcd for $C_{30}H_{20}S_2$ [M]+H, 445.1085; found, 445.1068.

Synthesis of compound 5
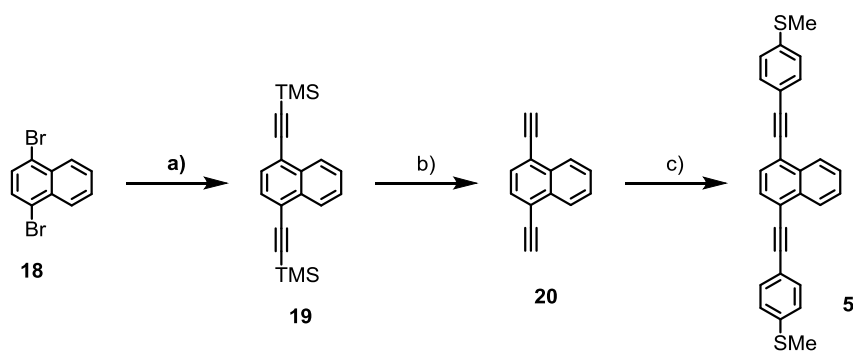
Scheme S1. Reagents and Conditions: (a) ethynyltrimethylsilane, PdCl$_2$(PPh$_3$)$_2$, CuI, DIPA, THF, reflux, 16 h 60%, (b) TBAF, DCM, rt, 1 h 90%, (c) 1-iodo-4-(methylsulfanyl)benzene, PdCl$_2$(PPh$_3$)$_2$, DIPA, THF, rt, 4 h 57%.

1,4-bis((trimethylsilyl)ethynyl)naphthalene (19)
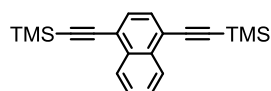
An oven-dried argon-flushed flask was charged with 1,4-dibromonaphthalene (**18**) (1.0 g, 3.5 mmol), PdCl$_2$(PPh$_3$)$_2$ (247 mg, 5 mol%), CuI (69 mg, 5 mol%) and dry THF (50 mL). The resulting mixture was degassed for 15 min followed by the addition of dry DIPA (10 mL). After further degassing for 5 min ethynyltrimethylsilane (1 mL, 690 mg, 7.03 mmol) was added and the reaction was stirred at reflux for 16 h. The reaction was then filtered through a pad of Celite^{TM}, and the residue was diluted in methylene chloride, washed sequentially with saturated aqueous NH$_4$Cl, water and brine. The organic layer was dried over MgSO$_4$ and removed at reduced pressure. The crude product was purified by flash column chromatography (SiO$_2$, hexane) affording **19** (674 mg, 2.10 mmol, 60%) as a white solid. ^{1}H NMR (400 MHz, CDCl$_3$, δ): 8.36–8.32 (m, 2H), 7.63 (s, 2H), 7.62–7.59 (m, 2H), 0.39 (s, 18H). ^{13}C NMR (101 MHz, CDCl$_3$, δ): 133.21, 130.12, 127.40, 126.69, 121.66, 102.91, 101.53. HRMS–ASAP–TOF (m/z): calcd for C$_{20}$H$_{24}$Si$_2$ [M]+H, 320.1417; found, 320.1414.

1,4-diethynylnaphthalene (20)
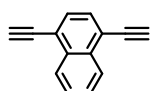
An oven-dried argon-flushed flask was charged with 1,4-bis((trimethylsilyl)ethynyl)naphthalene (**19**) (500 mg, 1.56 mmol), and methylene chloride

(50 mL). To the resulting mixture was added TBAF in THF (1 M, 7.5 mL, 7.5 mmol) and the reaction was stirred at rt for 1 h. After completion, the reaction mixture was washed with water and brine. The organic layer was dried over $MgSO_4$ and removed at reduced pressure affording **20** (248 mg, 1.41 mmol, 90%) as a white solid. ^{1}H NMR (400 MHz, $CDCl_3$, δ): 8.39–8.37 (m, 2H), 7.68 (s, 2H), 7.64–7.61 (m, 2H), 3.56 (s, 2H). ^{13}C NMR (101 MHz, $CDCl_3$, δ): 133.32,130.46, 127.62, 126.58, 121.09, 83.79, 81.54. HRMS–ASPA–TOF (m/z): calcd for $C_{14}H_9$ [M]+H, 177.0704; found, 177.0706.

1,4--bis(ethynyl-4-(methylsulfanyl)benzene)naphthalene (5)
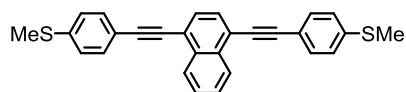
An oven-dried argon-flushed flask was charged with 1,4-diethynylnaphthalene (**20**) (200 mg, 1.13 mmol), $PdCl_2(PPh_3)_2$ (81 mg, 5 mol%), CuI (23 mg, 5 mol%) and dry THF (25 mL). The resulting mixture was degassed for 15 min followed by the addition of dry DIPA (5mL). After further degassing for 5 min 1-iodo-4-(methylsulfanyl)benzene (580 mg, 2.32 mmol) was added and reaction was stirred at rt for 4 h. The reaction was then filtered through a pad of Celite^{TM}, and the residue was diluted in methylene chloride, washed sequentially with saturated aqueous NH_4Cl, water and brine. The organic layer was dried over $MgSO_4$ and removed at reduced pressure. The crude product was purified by flash column chromatography (SiO_2, hexane/methylene chloride, 3:1 (v/v)) affording **5** (273 mg, 0.649 mmol, 57%) as a yellow solid, further purified by recrystallization from toluene/hexane. ^{1}H NMR (400 MHz, DMSO-d_6, δ): 7.46–7.43 (m, 2H), 7.82 (s, 2H), 7.88–7.77 (m, 2H), 7.67–7.64 (m, 4H), 7.37–7.34 (m, 4H), 2.54 (s, 6H) ^{13}C NMR (101 MHz, DMSO-d_6, δ): 140.38, 132.23, 131.97, 129.86, 128.09, 126.27, 125.67, 120.67, 117.94, 96.29, 87.18, 14.23. HRMS–ASAP–TOF (m/z): calcd for $C_{30}H_{20}S_2$ [M], $C_{28}H_{20}S_2$ 420.1006; found, 420.1002.

Synthesis of compound 6
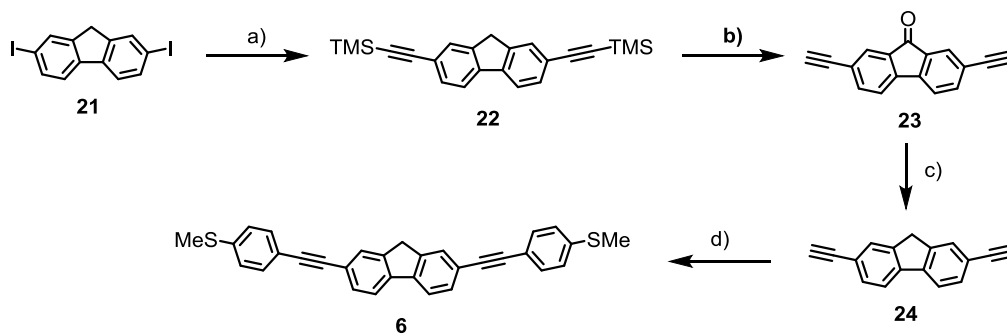
Scheme S2. Reagents and Conditions: (a) ethynyltrimethylsilane, $PdCl_2(PPh_3)_2$, CuI, DIPA, THF, rt, 2 h 78%, (b) TBAF, DCM, rt, 1 h 86%, (possibly accidental O_2 through air) (c) $N_2H_4 \cdot H_2O$, 100 °C, 16 h, then KOH, H_2O 100 °C, 1 h, 92% (d) 1-iodo-4-(methylsulfanyl)benzene, $PdCl_2(PPh_3)_2$, DIPA, THF, rt, 4 h, 69%.

2,7-bis((trimethylsilyl)ethynyl)fluorene (22)
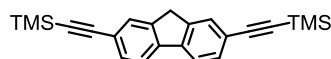
An oven-dried argon-flushed flask was charged with 2,7-diiodofluorene (300 mg, 0.72 mmol), $PdCl_2(PPh_3)_2$ (52 mg, 5 mol%), CuI (15 mg, 5 mol%) and dry THF (50 mL). The resulting mixture was degassed for 15 min followed by the addition of dry DIPA (10mL). After further degassing for 5 min, ethynyltrimethylsilane (0.25 mL, 172.5 mg, 1.76 mmol) was added and reaction was stirred at rt for 4 h. The reaction was then filtered through a pad of Celite^{TM}, and the residue was diluted in methylene chloride, washed sequentially with saturated aqueous NH_4Cl, water and brine. The organic layer was dried over $MgSO_4$ and removed at reduced pressure. The crude product was further purified by flash column chromatography (SiO_2, hexane) affording **22** (201 mg, 0.56 mmol, 78%) as a white solid. ^1H NMR (400 MHz, $CDCl_3$, δ): 7.68 (dm, J = 7.93, 2H), 7.64 (m, 2H), 7.49 (dm, J = 7.93 Hz, 2H), 3.84 (s, 2H)z. ^{13}C NMR (101 MHz, $CDCl_3$, δ): 143.53, 141.47, 131.15, 128.70, 121.74, 120.12, 105.81, 94.60, 36.59, 0.17. HRMS–ESI– (m/z): calcd for $C_{23}H_{26}Si_2$ [M], 358.1573; found, 358.1569.

2,7-diethynyl-9*H*-fluoren-9-one (23)
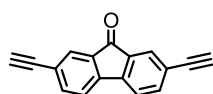
An oven-dried argon-flushed flask was charged with 2,7-bis((trimethylsilyl)ethynyl)fluorene (**22**) (180 mg, 0.5 mmol), and degassed dry methylene chloride (50 mL). Resulting mixture was added TBAF in THF (1 M, 2 mL, 2 mmol) and the reaction was stirred at rt for 1 h under argon (there may have been introduced O_2 through air). The reaction was washed with water and brine. The organic layer was dried over $MgSO_4$ and removed at reduced pressure affording **23** (98 mg, 0.43 mmol, 86%) as a yellow solid. ^1H NMR (400 MHz, $CDCl_3$, δ): 7.77 (dd, J = 1.6, 0.7 Hz, 2H), 7.63 (dd, J = 7.7, 1.6 Hz, 2H), 7.50 (dd, J = 7.7, 0.7 Hz, 2H), 3.19 (s, 2H). ^{13}C NMR (101 MHz, $CDCl_3$, δ): 192.05, 143.77, 138.63, 134.46, 134.46, 128.14, 123.60, 120.78, 82.69, 79.37. HRMS–ESI– (m/z): calcd for $C_{17}H_8O$ [M], 228.0575; found, 228.0576.

2,7-diethynylfluorene (24)
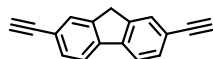
An oven-dried argon-flushed flask was charged with 2,7-diethynyl-9*H*-fluoren-9-one (**23**) (80 mg, 0.35 mmol), and degassed diethylene glycol (50 mL). To the resulting mixture was added $N_2H_4 \cdot H_2O$ (0.2 mL, 218 mg, 4.36 mmol) after which the reaction was stirred at 100 °C for 16 h under argon. KOH (100 mg, 1.78 mmol) dissolved in H_2O (1 mL) was added and stirred 1 h. The reaction was poured onto water (100 mL) and a crude product which precipitated was further purified by flash column chromatography (SiO_2, hexane) affording **24** (69 mg, 0.32 mmol, 92%) as a yellow solid. ^1H NMR (400 MHz, $CDCl_3$, δ): 7.75 (dd, *J* = 7.8, 0.8 Hz, 2H), 7.72–7.70 (m, 2H), 7.57–7.53 (m, 2H), 3.15 (s, 6H). HRMS–ESI– (m/z): calcd for $C_{17}H_{10}$ [M], 214.0783; found, 214.0787.

1,4-bis(ethynyl-4-(methylsulfanyl)benzene)-9*H*-fluorene (6)
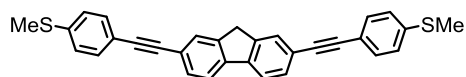
An oven-dried argon-flushed flask was charged with 2,7-diethynylfluorene (**24**) (60 mg, 0.28 mmol), $PdCl_2(PPh_3)_2$ (20.1 mg, 5 mol%), CuI (6.2 mg, 5 mol%) and dry THF (25 mL). The resulting mixture was degassed for 15 min followed by the addition of dry DIPA (5mL). After further degassing for 5 min, 1-iodo-4-(methylsulfanyl)benzene (150 mg, 0.60 mmol) was added and the reaction was stirred at rt for 4 h. The reaction was then filtered through a

pad of Celite^{TM}, and the residue was diluted in methylene chloride, washed sequentially with saturated aqueous NH$_4$Cl, water and brine. The organic layer was dried over MgSO$_4$ and removed at reduced pressure. The crude product was purified by flash column chromatography (SiO$_2$, hexane) affording **6** (89 mg, 0.19 mmol, 69%) as a yellow solid, further purified by recrystallization from toluene/hexane. ^{1}H NMR (400 MHz, CDCl$_3$, δ): 7.87 (d, J = 7.9 Hz, 2H), 7.70 (s, 2H), 7.53 (d, J = 7.9 Hz, 2H), 7.47 – 7.42 (dm, *J* = 8.4, 4H), 7.29 – 7.24 (dm, *J* = 8.4, 4H), 3.99 (s, 2H), 2.54 (s, 6H). ^{13}C NMR (101 MHz, CDCl$_3$, δ): 143.05, 140.38, 139.09, 131.15, 129.94, 127.46, 125.49, 123.88, 121.12, 119.89, 90.11, 89.58, 36.05, 14.62. HRMS–ESI– (m/z): calcd for C$_{31}$H$_{22}$S$_2$ [M], 458.1154; found, 4581149.

Synthesis of compound 7
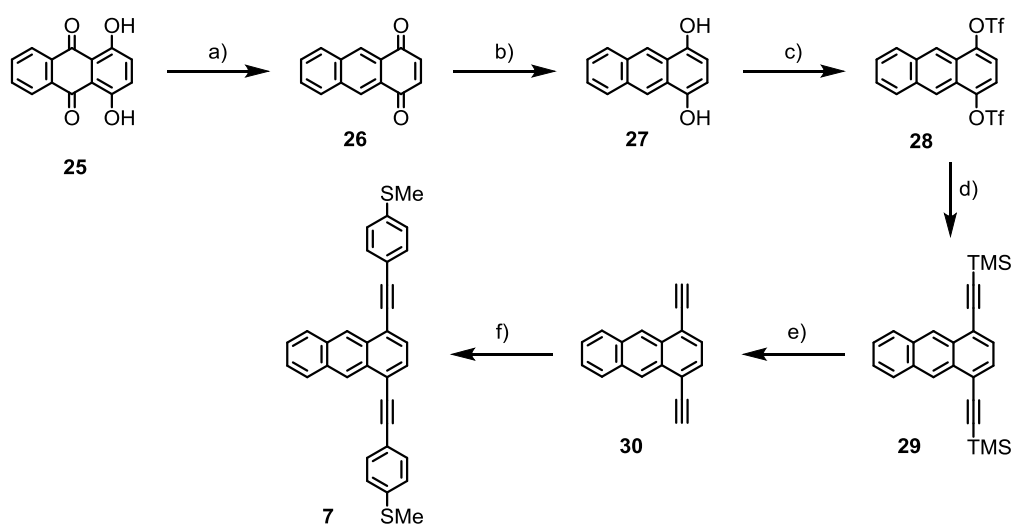
Scheme S3. Reagents and Conditions: (a) NaBH$_4$, MeOH, 0 °C, 1 h, then HCl (6 M), 0 °C, 10 min, 92%, (b) Na$_2$S$_2$O$_4$, H$_2$O, 1,4-dioxane, rt, 4 h, 79%, (c) Tf$_2$O, TEA, DCM, 2 h, rt, 90%, (d), ethynyltrimethylsilane, PdCl$_2$(PPh$_3$)$_2$, CuI, DIPA, THF, rt, 16 h 67%, (e) TBAF, DCM, rt, 1 h 95%, (f) 1-iodo-4-(methylsulfanyl)benzene, PdCl$_2$(PPh$_3$)$_2$, DIPA, THF, rt, 4h 54%.

Compound **27** was synthesized according to a literature procedure. Its ^{1}H- and ^{13}C-NMR spectra matched previously reported data.[11]

1,4-bis(trifluoromethanesulfonyl)anthracene (28)
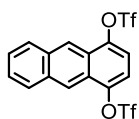
An oven-dried argon-flushed flask was charged with 1,4-dihydroxyanthracene **27** (1.0 g, 4.76 mmol), dry DCM (50 mL) and dry triethylamine (10 mL). The resulting mixture was degassed for 15 min followed by the dropwise addition of triflic anhydride (2 mL, 3.35 g, 11.9 mmol) and the reaction was stirred at rt for 2 h. The reaction was then quenched by the addition of H_2O and diluted with methylene chloride. The organic layer was dried over $MgSO_4$ and removed at reduced pressure. The crude product was purified by flash column chromatography (SiO_2, hexane) affording **28** (2.04 g, 4.30 mmol, 90%) as a yellow solid. ^{1}H NMR (400 MHz, $CDCl_3$, δ): 8.71 (s, 2H), 8.16–8.12 (m, 2H), 7.69–7.65 (m, 2H), 4.47 (s, 2H). ^{13}C NMR (101 MHz, $CDCl_3$, δ):145.07, 144.19, 139.33, 133.03, 128.78, 128.24, 121.39, 115.70, 46.48. HRMS–ASAP–TOF (m/z): calcd for $C_{16}H_8O_6F_6S_2$ [M], 473.9667; found, 473.9644.

1,4-bis((trimethylsilyl)ethynyl)anthracene (29)
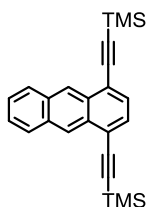
An oven-dried argon-flushed flask was charged with 1,4-bis(trifluoromethanesulfonyl)anthracene (**28**) (1.80 g, 3.79 mmol), $PdCl_2(PPh_3)_2$ (266 mg, 5 mol%), CuI (74 mg, 5 mol%) and dry THF (50 mL). The resulting mixture was degassed for 15 min followed by the addition of dry DIPA (10 mL). After further degassing for 5 min, ethynyltrimethylsilane (1.2 mL, 828 mg, 8.43 mmol) was added and the reaction was stirred at rt for 16 h. The reaction was filtered through a pad of Celite[TM], and the residue was diluted in methylene chloride, washed sequentially with saturated aqueous NH_4Cl, water and brine. The organic layer was dried over $MgSO_4$ and removed at reduced pressure. The crude product was purified by flash column chromatography (SiO_2, hexane) affording **29** (942 mg, 2.54 mmol, 67%) as a yellow solid. ^{1}H NMR (400 MHz, $CDCl_3$, δ): 8.90 (s, 2H), 8.09–8.07 (m, 2H), 7.64 (s, 2H), 7.55–7.52 (m, 2H), 0.39 (s, 18H). ^{13}C NMR (101 MHz, $CDCl_3$, δ):132.31, 130.65, 129.86, 128.64, 126.35, 125.87, 121.83, 103.22, 102.03, 0.29. HRMS–ASAP–TOF (m/z): calcd for $C_{24}H_{26}Si_2$ [M], 370.1573; found, 370.1561.

1,4-diethynylanthracene (30)
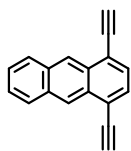
An oven-dried argon-flushed flask was charged with 1,4-bis((trimethylsilyl)ethynyl)anthracene (**29**) (900 mg, 2.43 mmol), and methylene chloride (50 mL). To the resulting mixture was added TBAF in THF (1 M, 10 mL, 10 mmol) and the reaction was stirred at rt for 1 h. The reaction was then washed with water and brine. The organic layer was dried over $MgSO_4$ and removed at reduced pressure affording **30** (521 mg, 2.30 mmol, 95%) as a yellow solid. ^1H NMR (400 MHz, $CDCl_3$, δ): 8.95 (s, 2H), 8.10–8.08 (m, 2H), 7.69 (s, 2H), 7.56–7.53 (m, 2H), 3.68 (s, 2H). HRMS–ASAP–TOF (m/z): calcd for $C_{18}H_{10}$ [M], 226.0783; found, 226.0785.

2,7-bis(ethynyl-4-(methylsulfanyl)benzene)anthracene (7)
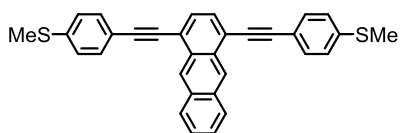
An oven-dried argon-flushed flask was charged with 1,4-diethynylanthracene (**30**) (250 mg, 1.1 mmol), $PdCl_2(PPh_3)_2$ (78 mg, 5 mol%), CuI (22 mg, 5 mol%) and dry THF (25 mL). The resulting mixture was degassed for 15 min followed by the addition of dry DIPA (5mL). After further degassing for 5 min, 1-iodo-4-(methylsulfanyl)benzene (555 mg, 2.22 mmol) was added and the reaction was stirred at rt for 4 h. The reaction was then filtered through a pad of Celite^{TM}, and the residue was diluted in methylene chloride, washed sequentially with saturated aqueous NH_4Cl, water and brine. The organic layer was dried over $MgSO_4$ and removed at reduced pressure. The crude product was purified by flash column chromatography (SiO_2, hexane/methylene chloride, 3:1 (v/v)) affording **7** (218 mg, 0.60 mmol, 54%) as a yellow solid which was further purified by recrystallization from toluene/hexane. ^1H NMR (400 MHz, $CDCl_3$, δ): 9.03 (s, 2H), 8.16–8.13 (m, 2H), 7.76 (s, 2H), 7.67–7.64 (m, 4H), 7.59–7.56 (m, 2H), 7.34–7.31 (m, 4H), 2.58 (s, 6H). ^{13}C NMR (101 MHz, DMSO-d_6/CS_2, δ): 140.82, 132.26, 131.73, 129.56, 127.59, 126.24, 125.50, 120.78, 118.13, 114.00, 87.44, 84.21, 14.47. HRMS–ASAP–TOF (m/z): calcd for $C_{32}H_{22}S_2$ [M], 470.1163; found, 470.1143.

Synthesis of compound 8
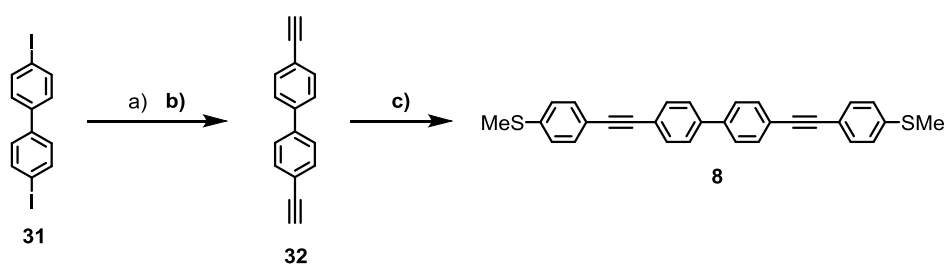
Scheme S4. Reagents and Conditions: (a) ethynyltrimethylsilane, PdCl$_2$(PPh$_3$)$_2$, CuI, DIPA, THF, reflux, 16 h, (b) TBAF, DCM, rt, 1 h 63% for the two steps, (c) 1-iodo-4-(methylsulfanyl)benzene, PdCl$_2$(PPh$_3$)$_2$, DIPA, THF, rt, 4 h 63%.

4,4'-diethynyl-1,1'-biphenyl (32)
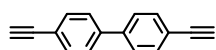
An oven-dried argon-flushed flask was charged with 4,4'-diiodo-1,1'-biphenyl **31** (500 mg, 1.23 mmol), PdCl$_2$(PPh$_3$)$_2$ (88.2 mg, 5 mol%), CuI (25.1 mg, 5 mol%) and dry THF (100 mL). Resulting mixture was degassed for 15 min followed by the addition of dry DIPA (10mL). After further degassing for 5 min, ethynyltrimethylsilane (0.4 mL, 276 mg, 2.81 mmol) was added and the reaction was stirred at reflux for 16 h. The reaction was then filtered through a pad of Celite^{TM}, and the residue was diluted in methylene chloride, washed sequentially with saturated aqueous NH$_4$Cl, water and brine. To the organic layer was added TBAF in THF (1 M, 10 mL, 10 mmol) and the reaction was stirred at rt for 1 h. The reaction was washed with water and brine. The organic layer was dried over MgSO$_4$ and removed at reduced pressure. The crude product was purified by flash column chromatography (SiO$_2$, hexane) affording **32** (156 mg, 0.772 mmol, 63%) as a white solid. ^{1}H NMR (400 MHz, CDCl$_3$, δ): 7.58–7.53 (m, 8H), 3.14 (s 2H). ^{13}C NMR (101 MHz, CDCl$_3$, δ): 140.68, 132.79, 127.05, 121.61, 83.51, 78.24. HRMS–ASAP–TOF (m/z): calcd for C$_{16}$H$_{10}$ [M], 202.0783; found, 202.0793.

4,4'-bis(ethynyl-4-(methylsulfanyl)benzene)-1,1'-biphenyl (8)
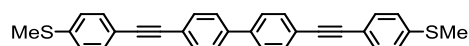
An oven-dried argon-flushed flask was charged with 4,4'-diethynyl-1,1'-biphenyl (**32**) (100 mg, 0.49 mmol), PdCl$_2$(PPh$_3$)$_2$ (35.2 mg, 5 mol%), CuI (11.1 mg, 5 mol%) and dry THF (25

mL). Resulting mixture was degassed for 15 min followed by the addition of dry DIPA (5mL). After further degassing for 5 min, 1-iodo-4-(methylsulfanyl)benzene (260 mg, 1.04 mmol) was added and reaction was stirred at rt for 4 h. The reaction was filtered through a pad of Celite^{TM}, and the residue was diluted in methylene chloride, washed sequentially with saturated aqueous NH_4Cl, water and brine. The organic layer was dried over $MgSO_4$ and removed at reduced pressure. The crude product was further purified by flash column chromatography (SiO_2, hexane//methylene chloride, 3:1 (v/v)) affording **8** (148 mg, 0.772 mmol, 63%) as a yellow solid, further purified by recrystallization from toluene/hexane. ^{1}H NMR (400 MHz, DMSO-d_6/CS$_2$ 1:1(v/v) δ): 7.69 (d, J = 8.0 Hz, 2H), 7.58 (d, J = 8.0 Hz, 2H) 7.44 (d, J = 8.0 Hz, 2H) 7.26 (d, J = 8.0 Hz, 2H), 2.52 (s, 6H). ^{13}C NMR (101 MHz, DMSO-d_6/CS$_2$ 1:1 v/v, δ): 139.32, 138.83, 131.41, 126.28, 125.49, 123.88, 121.86, 118.47, 90.21, 89.16, 14.55. HRMS–ASAP–TOF (m/z): calcd for $C_{30}H_{22}S_2$ [M], 446.1163; found, 446.1164.

4. Copies of NMR spectra of Compounds 1-8

^{1}H NMR and ^{13}C NMR Spectra of 1

Figure S9: ^{1}H NMR Spectrum of **1** in CDCl$_3$ (δ CHCl$_3$ 7.26)
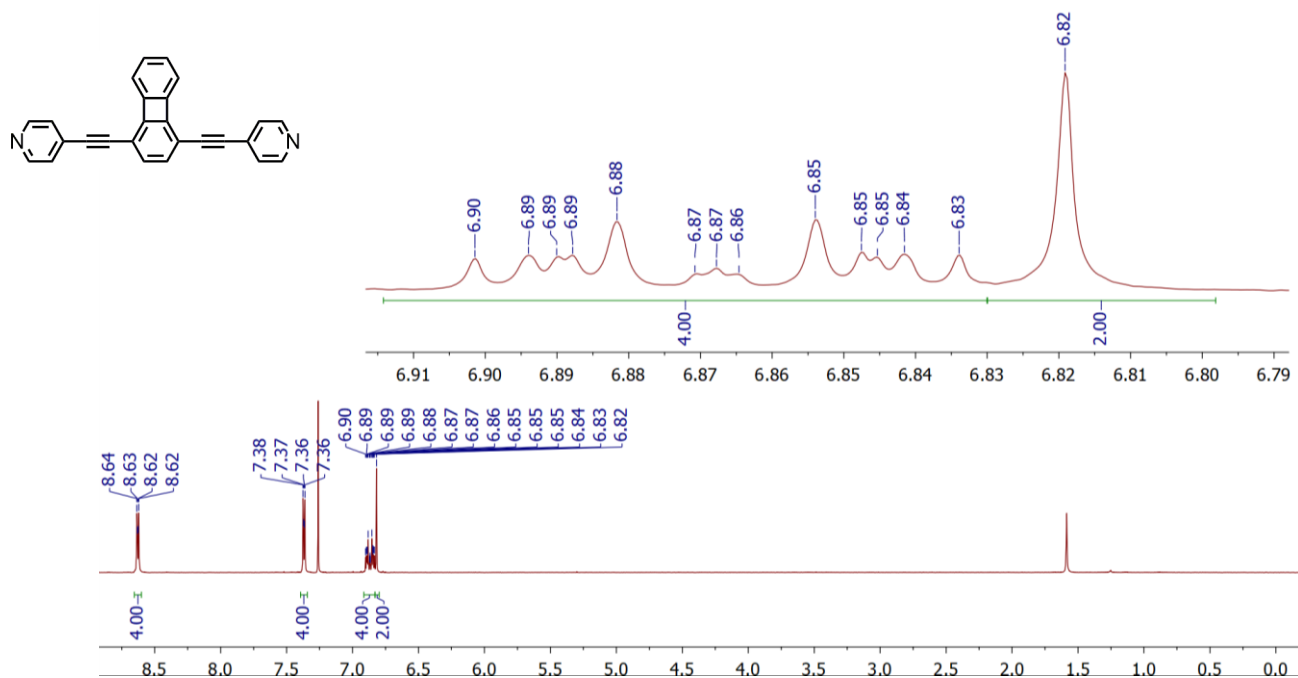
Figure S10: ^{13}C NMR Spectrum of **1** in CDCl$_3$ (δ 77.16)
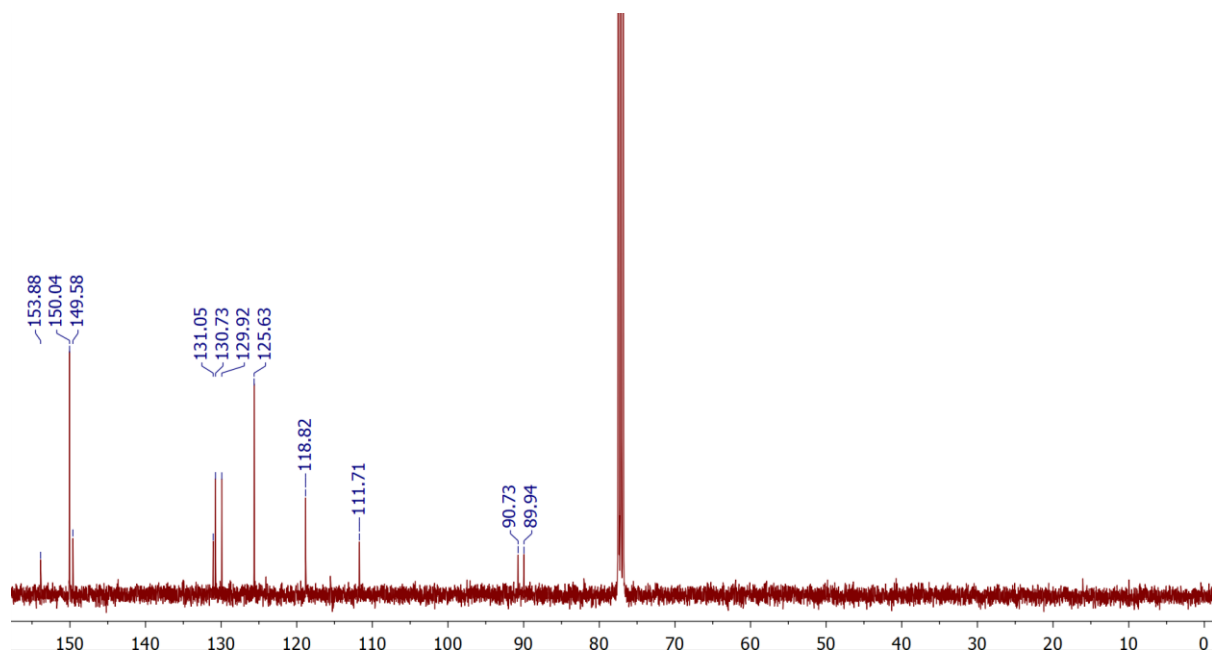
^{1}H NMR and ^{13}C NMR Spectra of 2

Figure S11: ^{1}H NMR Spectrum of **2** in CDCl$_3$ (δ CHCl$_3$ 7.26)
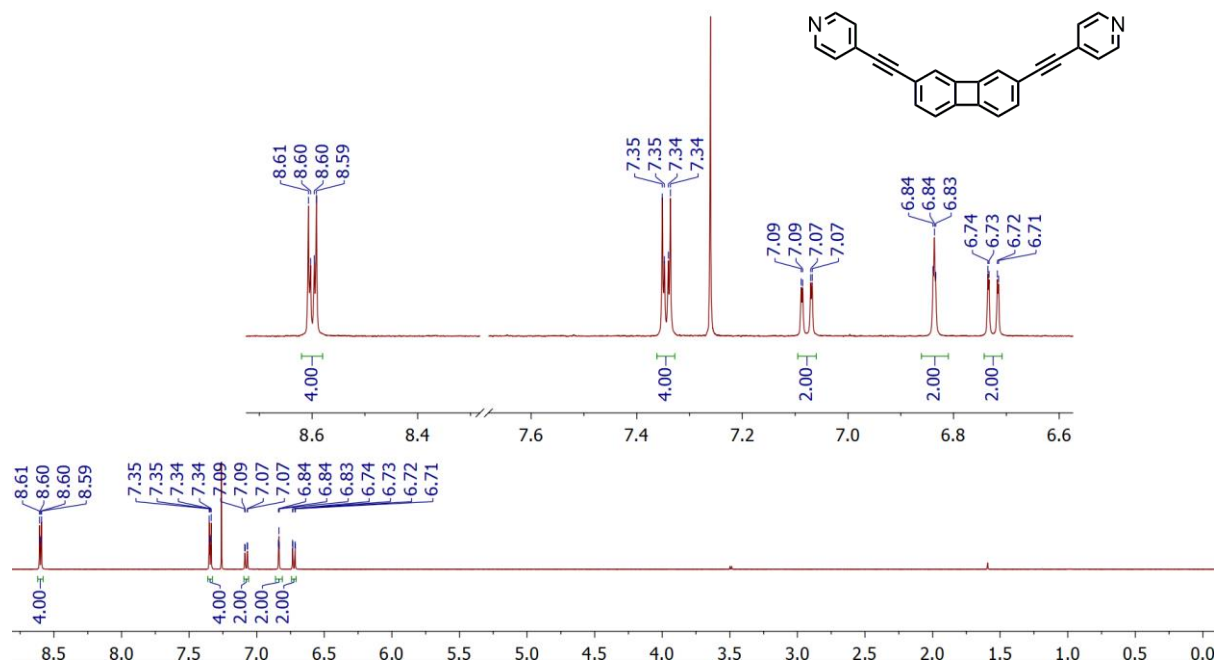
Figure S12: ^{13}C NMR Spectrum of **2** in CDCl$_3$ (δ 77.16)
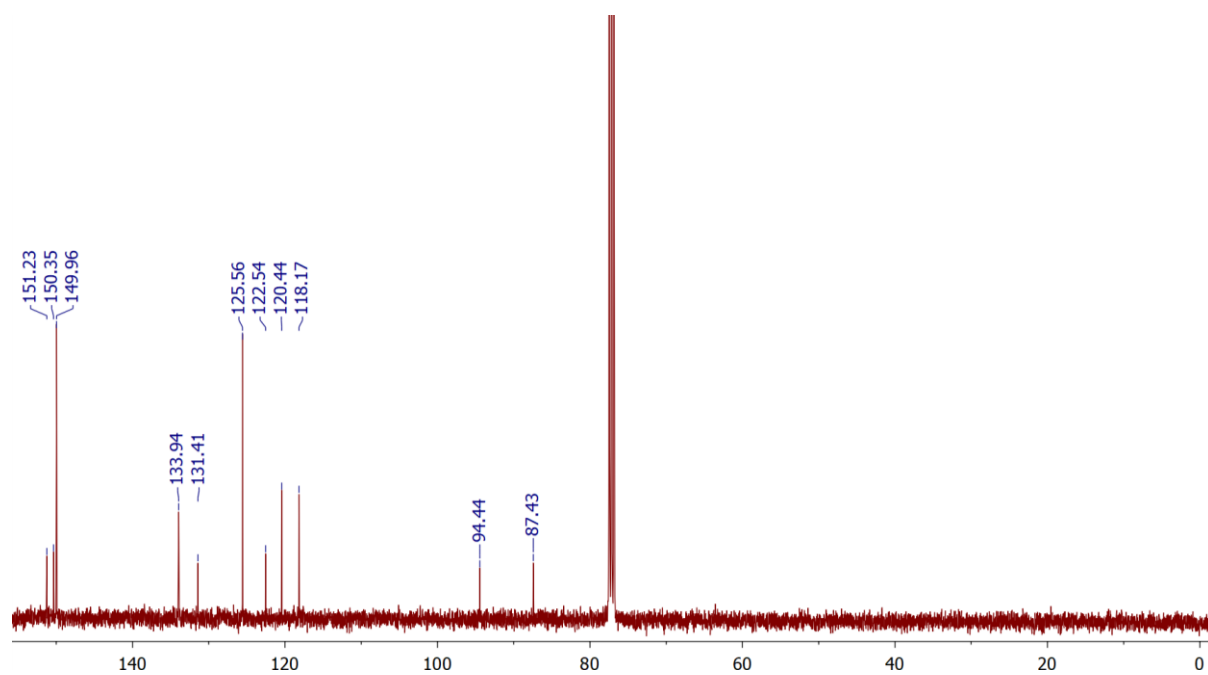
^{1}H NMR and ^{13}C NMR Spectra of 3

Figure S13: ^{1}H NMR Spectrum of **3** in Acetone-d_6 (δ Acetone 2.05)
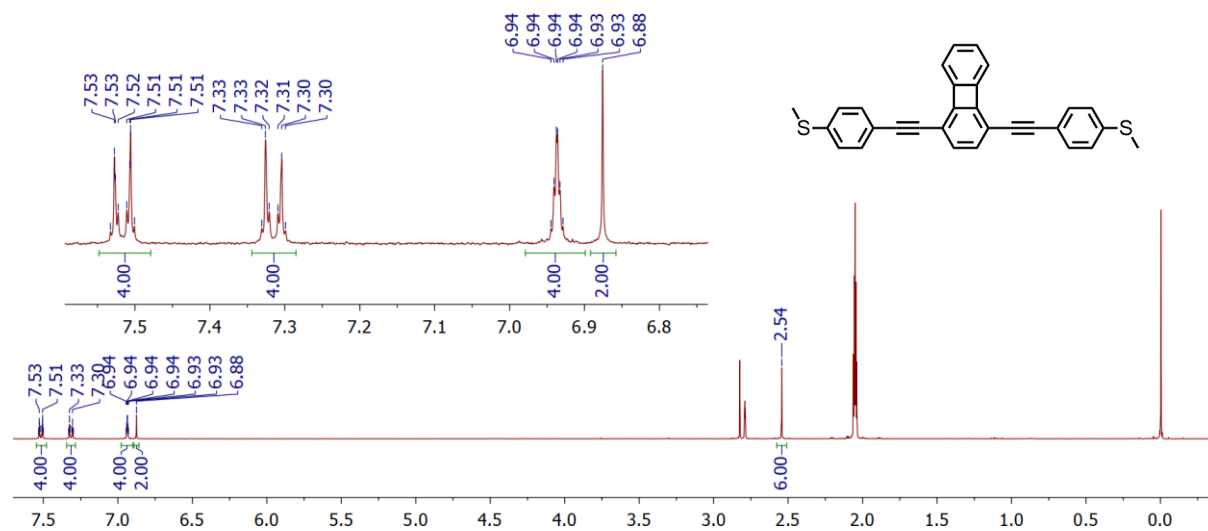
Figure S14: ^{13}C NMR Spectrum of **3** in CDCl$_3$ (δ 77.16)
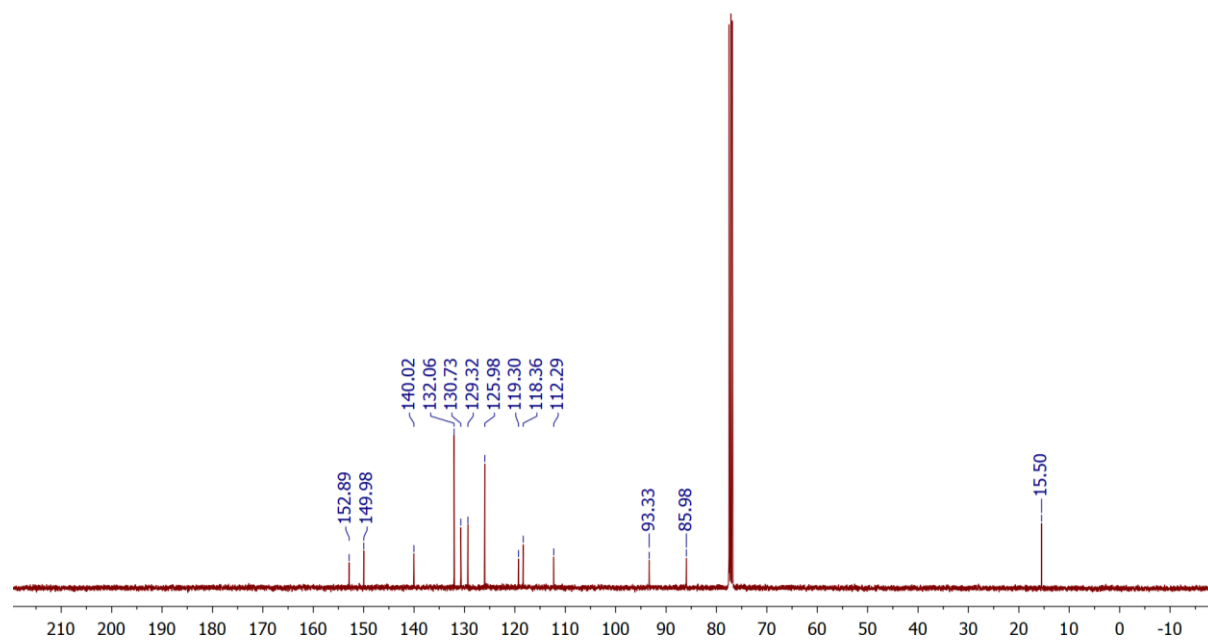
^{1}H NMR and ^{13}C NMR Spectra of 4

Figure S1: ^{1}H NMR Spectrum of **4** in CDCl$_3$ (δ CHCl$_3$ 7.26)
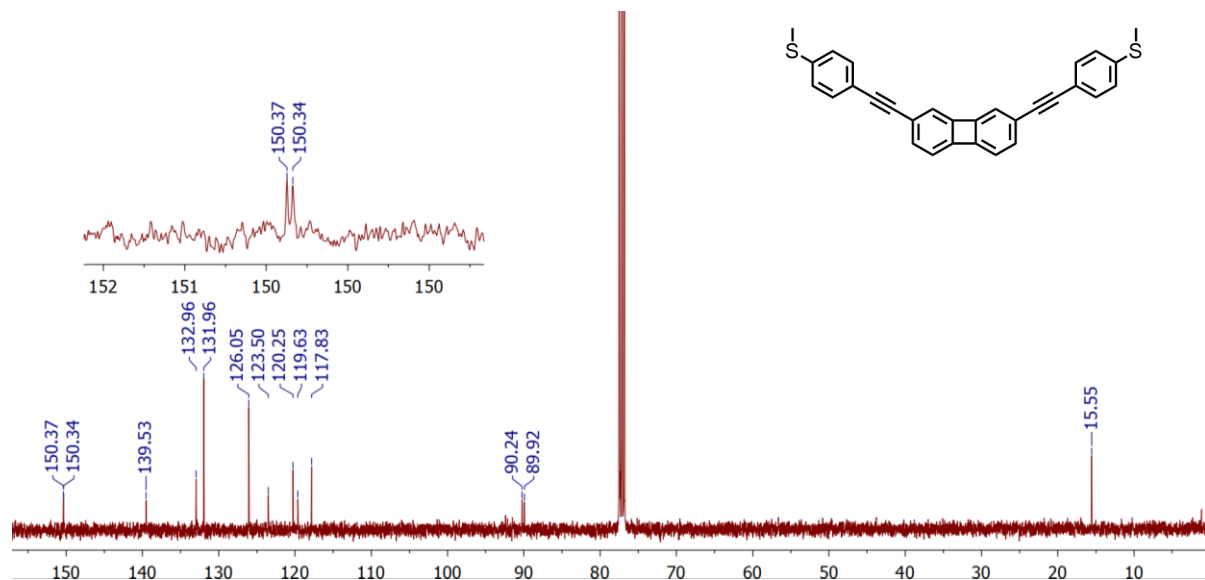
Figure S2: ^{13}C NMR Spectrum of **4** in CDCl$_3$ (δ 77.16)
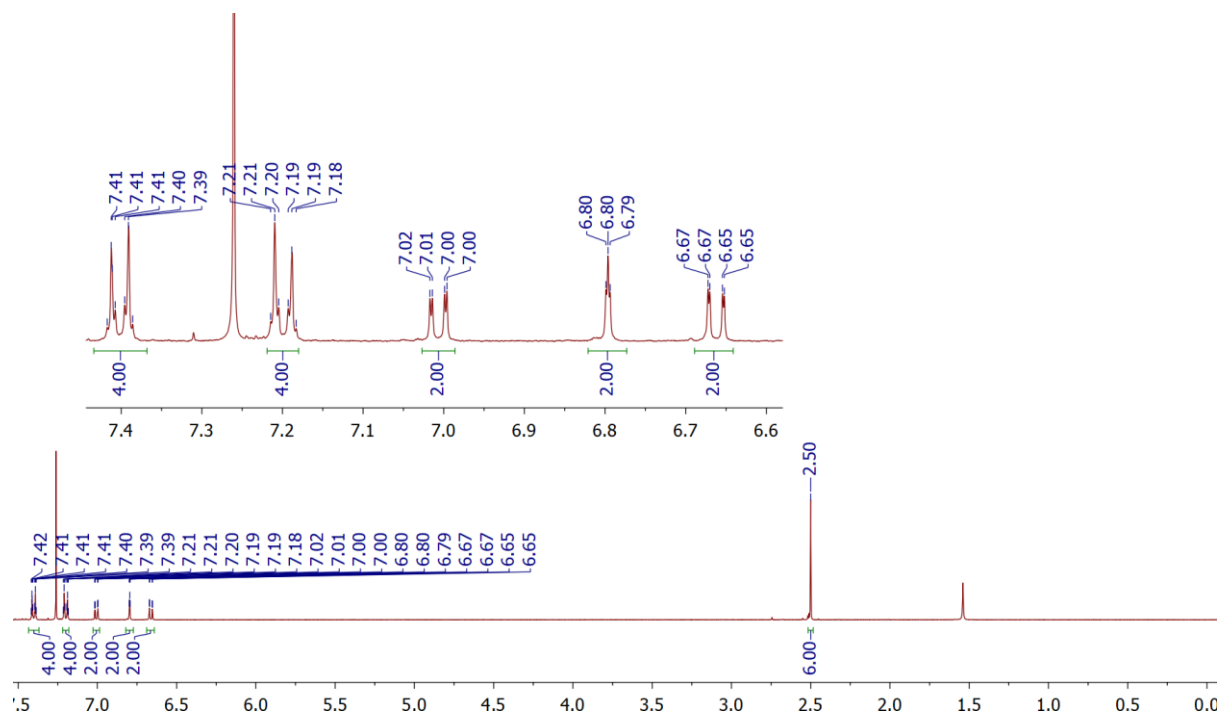
^{1}H NMR and ^{13}C NMR Spectra of 5

Figure S17: ^{1}H NMR Spectrum of **5** in DMSO-d_6 (δ DMSO 2.50)
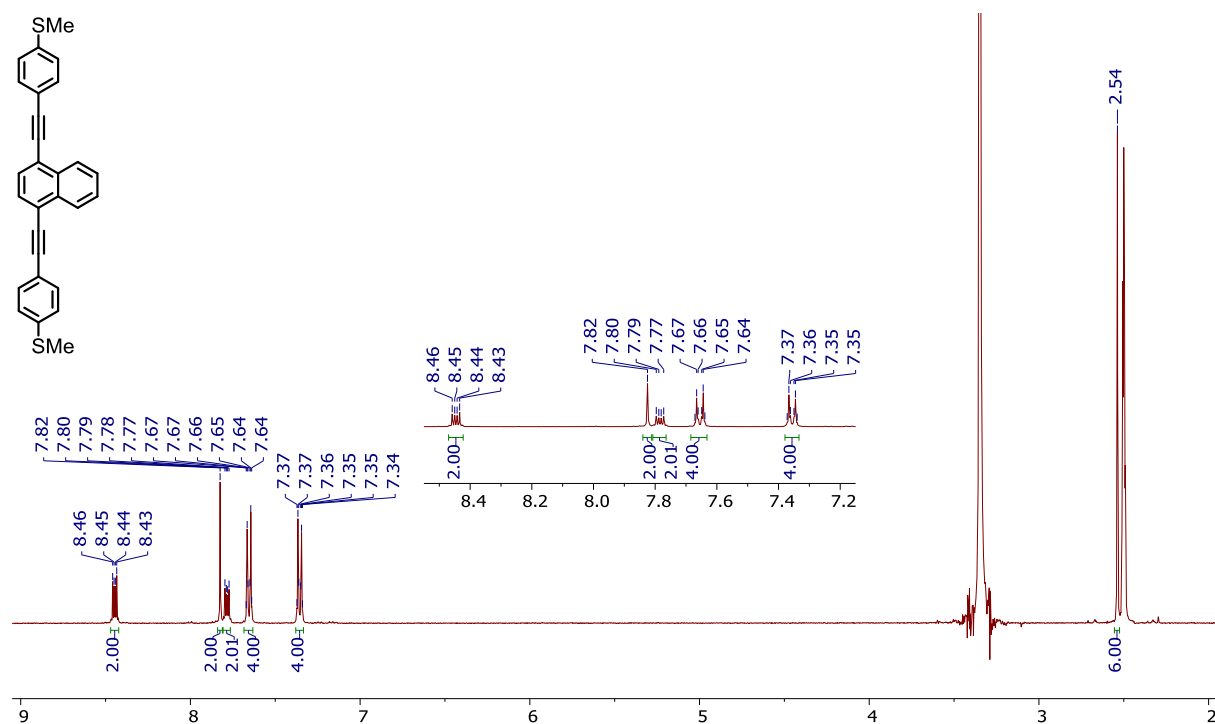
Figure S18: ^{13}C NMR Spectrum of **5** in DMSO-d_6 (δ 39.52)
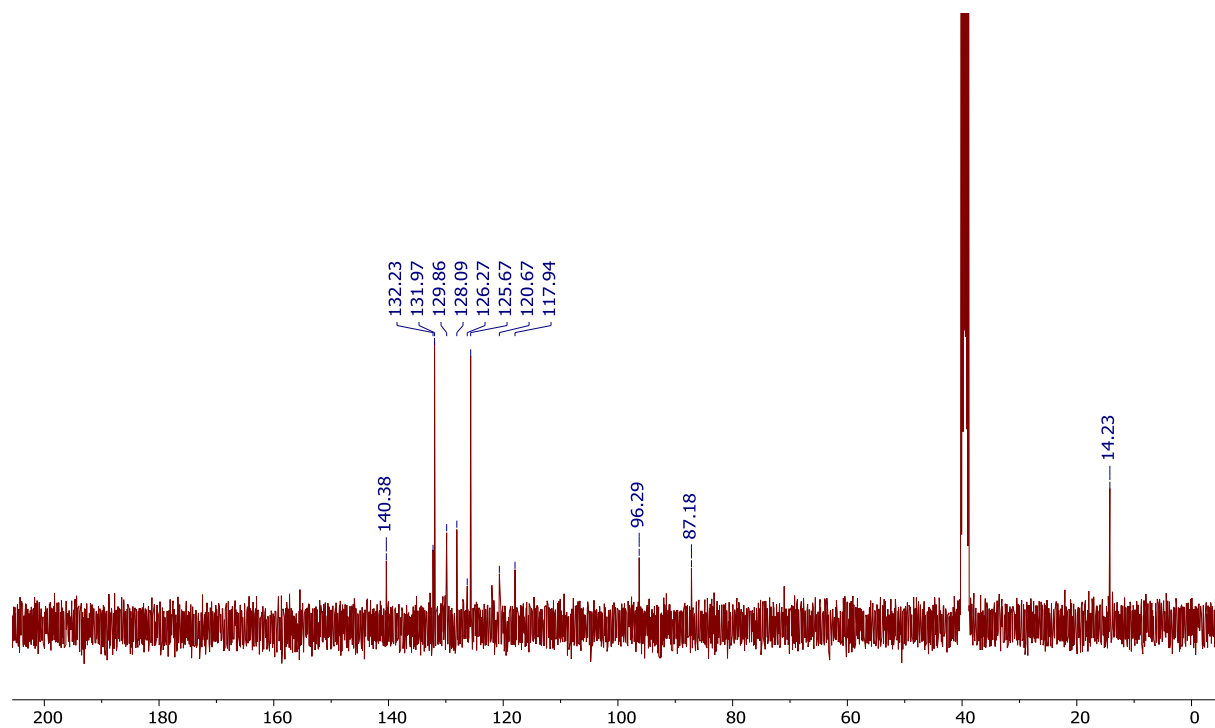
^{1}H NMR and ^{13}C NMR Spectra of 6

Figure S19: ^{1}H NMR Spectrum of **6** in DMSO-d_6 (δ DMSO 2.50)
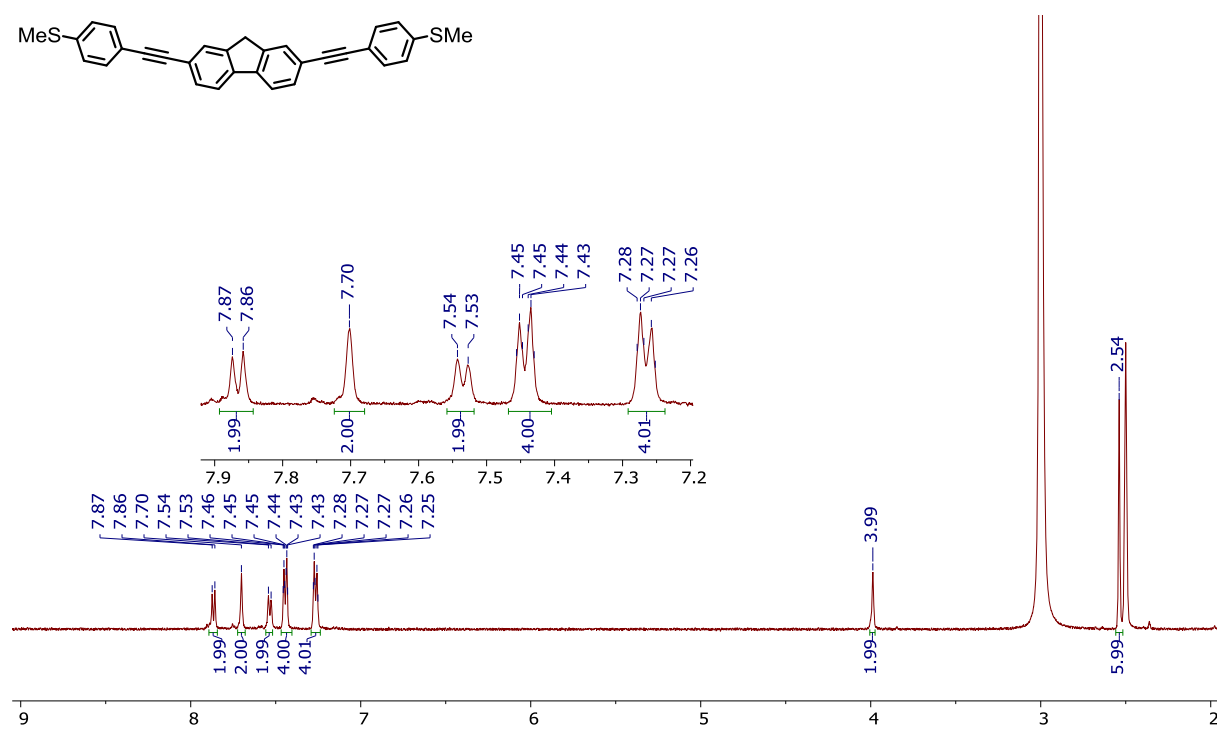
Figure S20: ^{13}C NMR Spectrum of **6** in DMSO-d_6/CS$_2$ 1:1 (v/v) (δ DMSO 39.52, CS$_2$ 191.96)

^{1}H NMR and ^{13}C NMR Spectra of 7

Figure S21: ^{1}H NMR Spectrum of **7** in CDCl$_3$ (δ CHCl$_3$ 7.26)

Figure S22: ^{13}C NMR Spectrum of **7** in DMSO-d_6/CS$_2$ 1:1 (v/v) (δ DMSO 39.52, CS$_2$ 192.43)
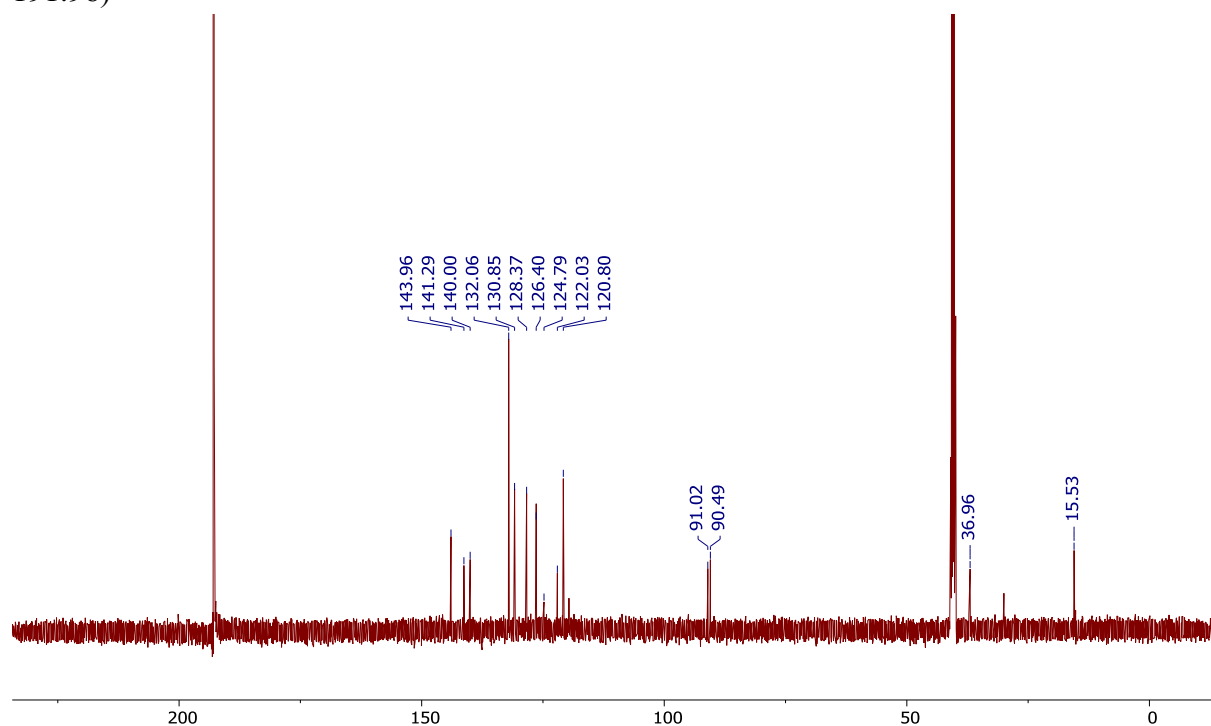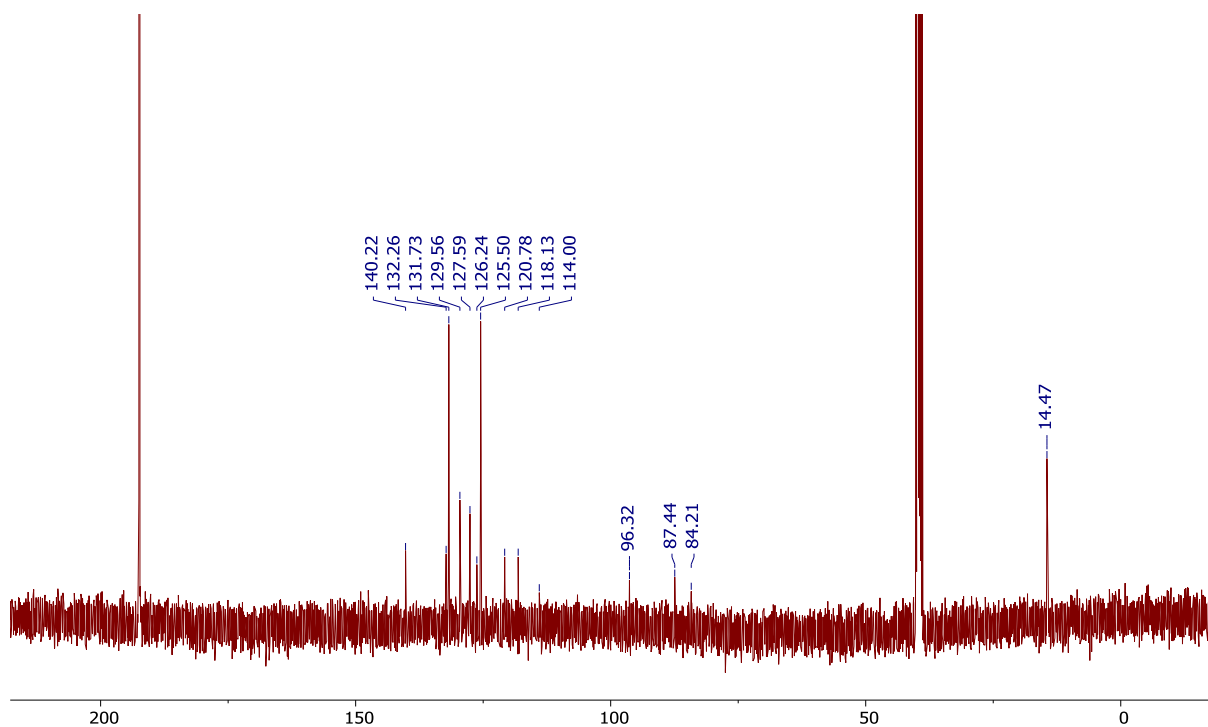
Figure S23: ^{1}H NMR Spectrum of **8** in DMSO-d_6/CS$_2$ 1:1 (v/v) (DMSO δ 2.50)
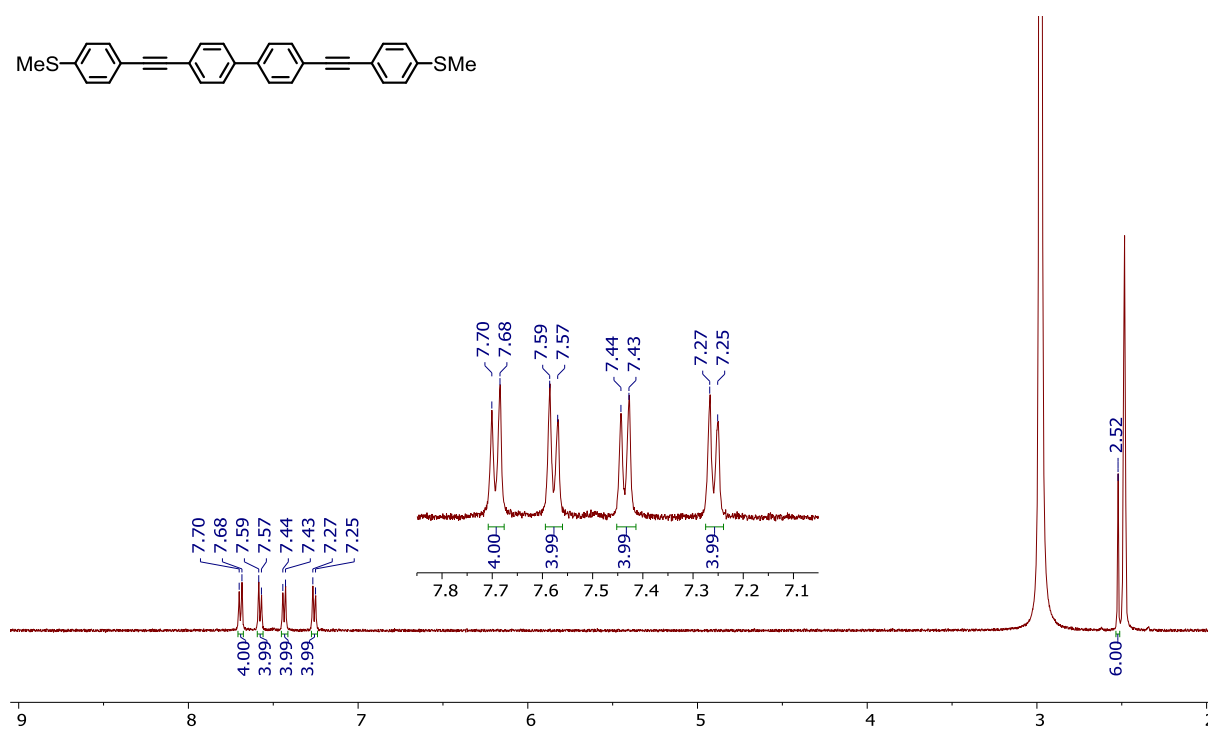
Figure S24: ^{13}C NMR Spectrum of **8** in DMSO-d_6/CS$_2$ 1:1 (v/v) (δ DMSO 39.52, CS$_2$ 192.01)
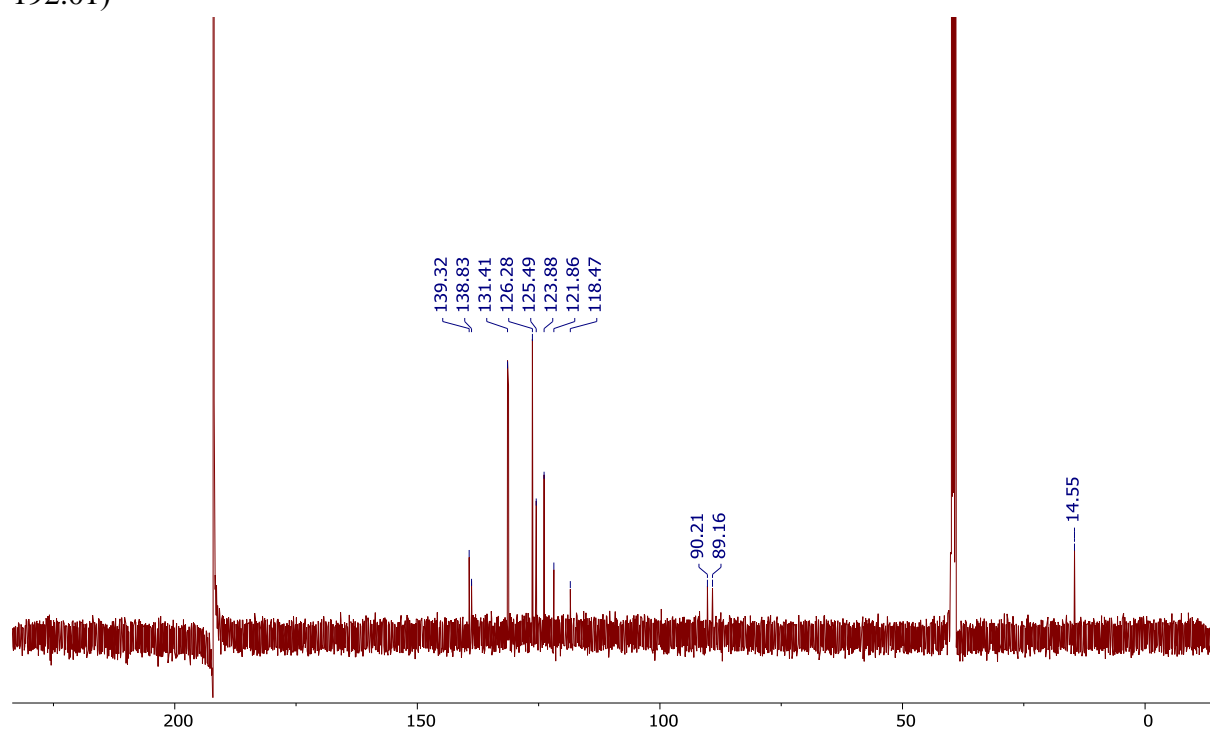
5. Copies of NMR Spectra of Synthetic Intermediates

^{1}H NMR and ^{13}C NMR Spectra of 11

Figure S25: ^{1}H NMR Spectrum of **11** in Acetone-d$_6$ (δ Acetone 2.05)
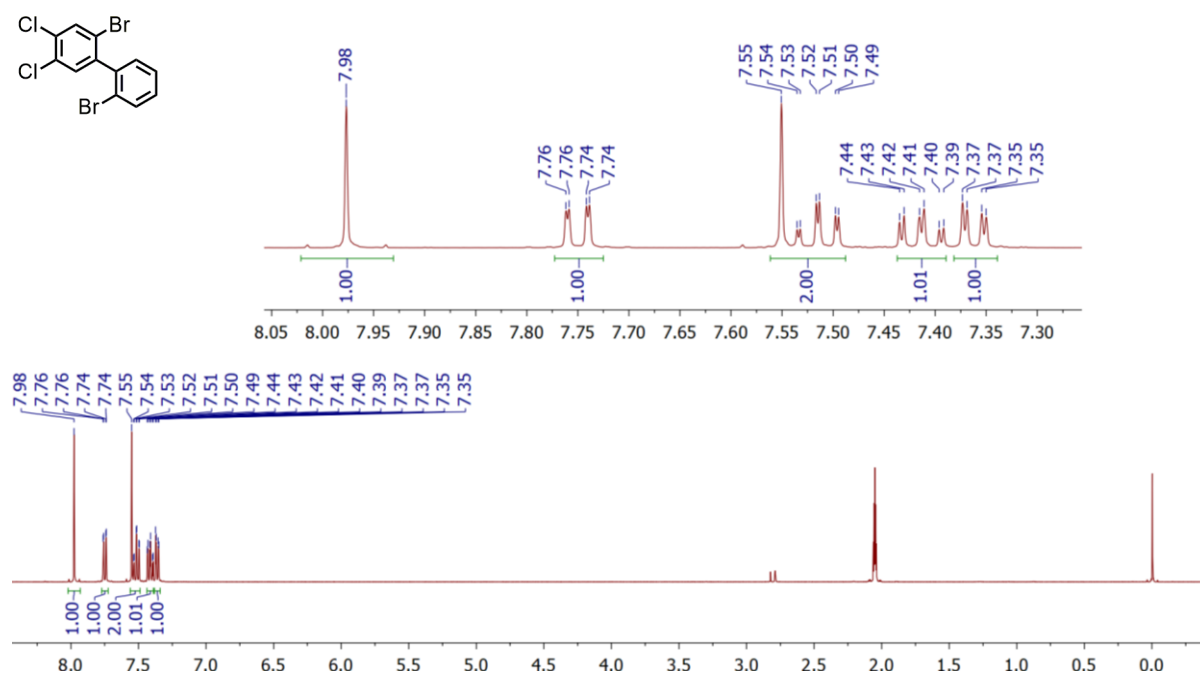
Figure S26: ^{13}C NMR Spectrum of **11** in Acetone-d$_6$ (δ Acetone 29.84)
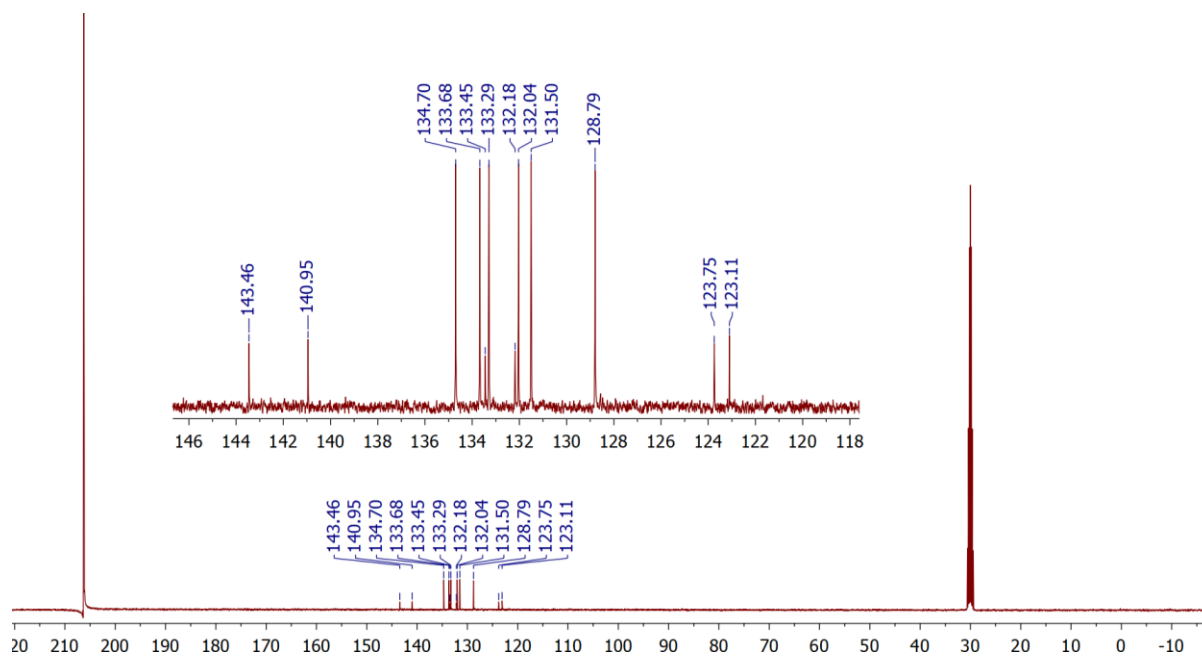
^{1}H NMR and ^{13}C NMR Spectra of 12

Figure S27: ^{1}H NMR Spectrum of **12** in Acetone-d$_6$ (δ Acetone 2.05)
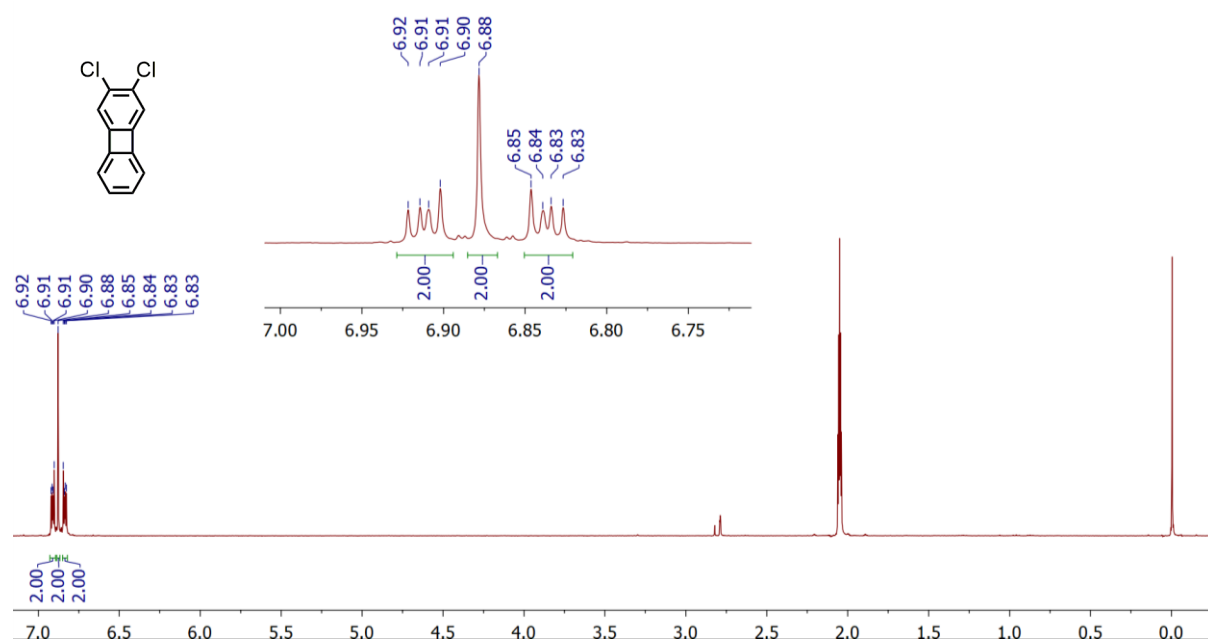
Figure S28: ^{13}C NMR Spectrum of **12** in Acetone-d$_6$ (δ Acetone 29.84)
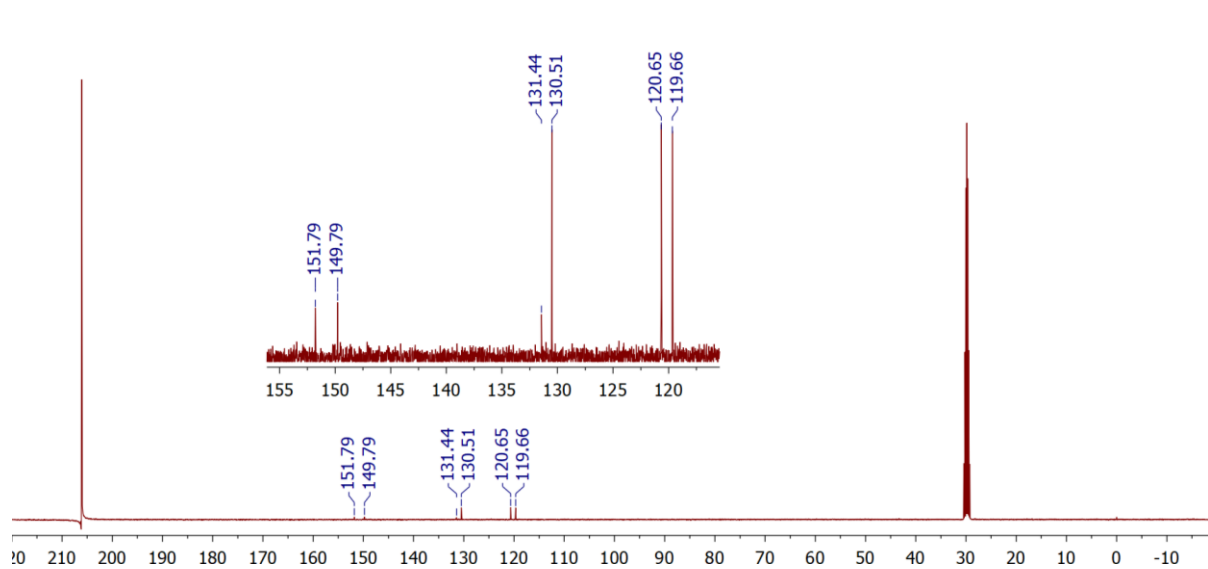
^{1}H NMR and ^{13}C NMR Spectra of 13

Figure S29: ^{1}H NMR Spectrum of **13** in CDCl$_3$ (δ CHCl$_3$ 7.26)
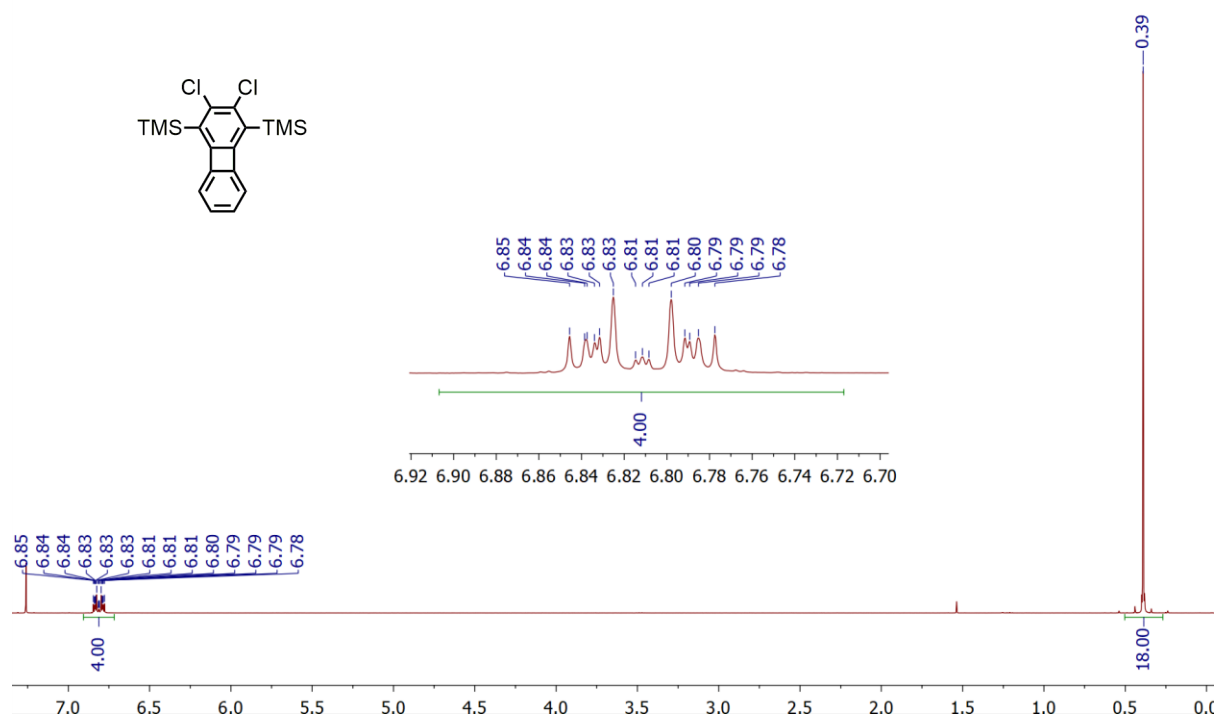
Figure S30: ^{13}C NMR Spectrum of **13** in CDCl$_3$ (δ 77.16)
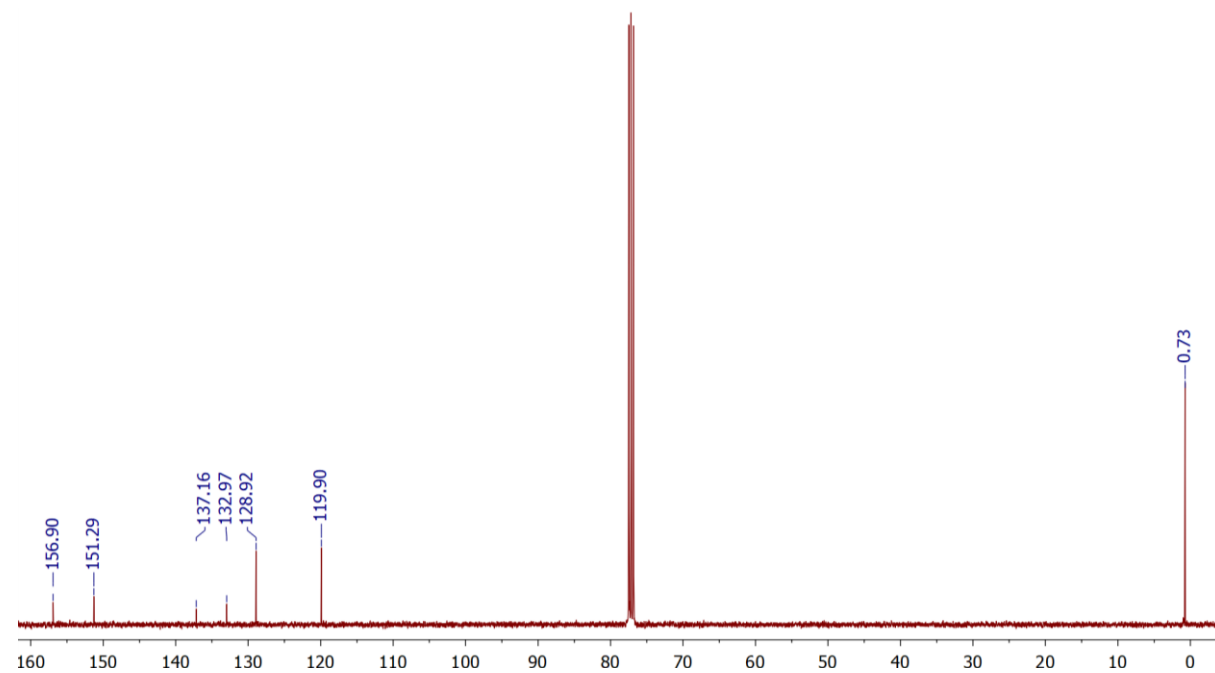
^{1}H NMR and ^{13}C NMR Spectra of 14

Figure S31: ^{1}H NMR Spectrum of **14** in Acetone-d$_6$ (δ Acetone 2.05)
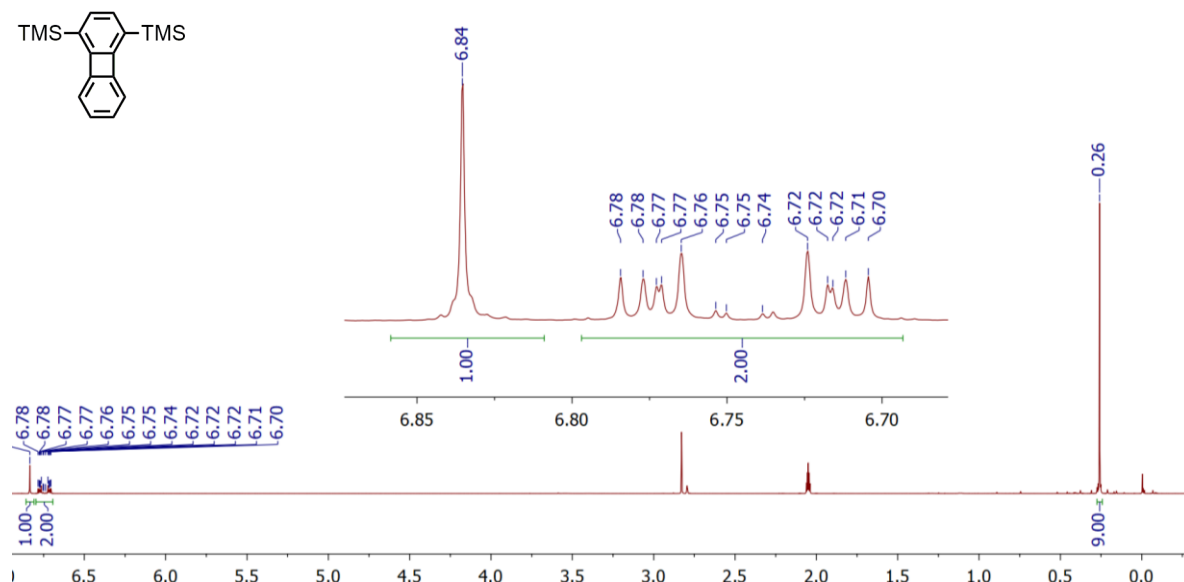
Figure S32: ^{13}C NMR Spectrum of **14** in Acetone-d$_6$ (δ Acetone 29.84)
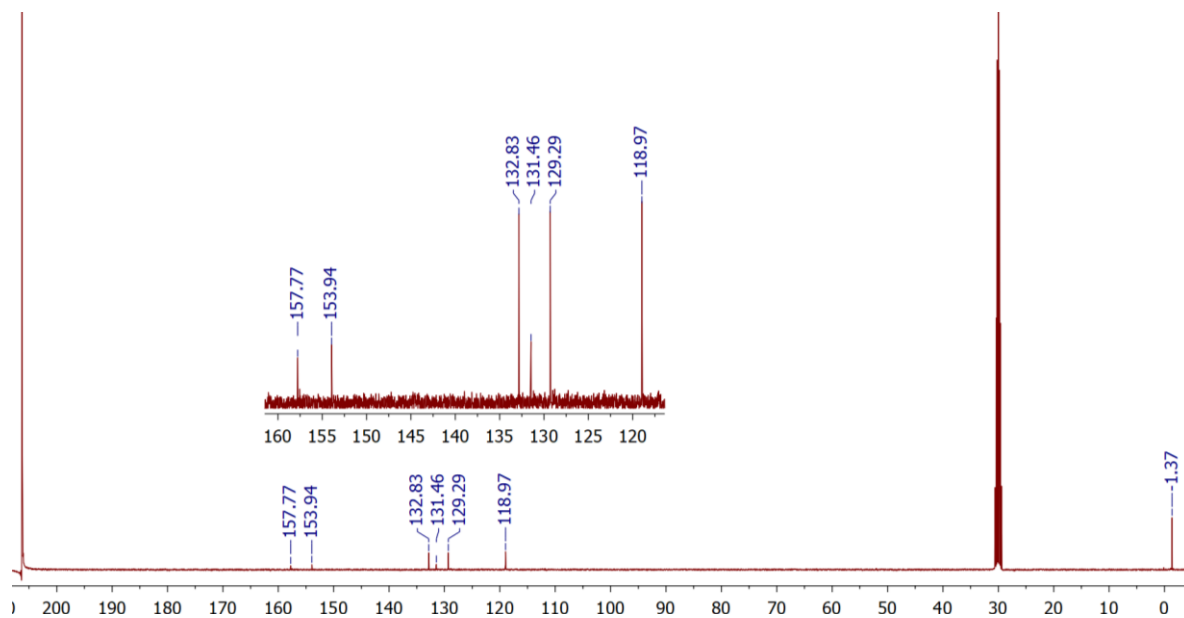
^{1}H NMR and ^{13}C NMR Spectra of 15

Figure S33: ^{1}H NMR Spectrum of **15** in CDCl$_3$ (δ CHCl$_3$ 7.26)
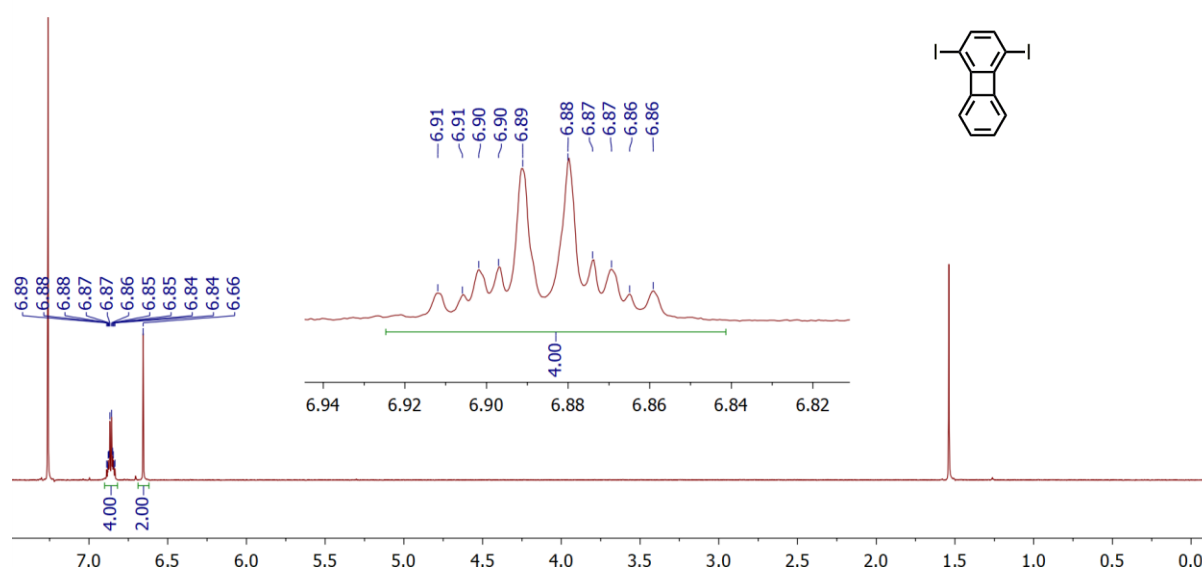
Figure S34: ^{13}C NMR Spectrum of **15** in CDCl$_3$ (δ 77.16)
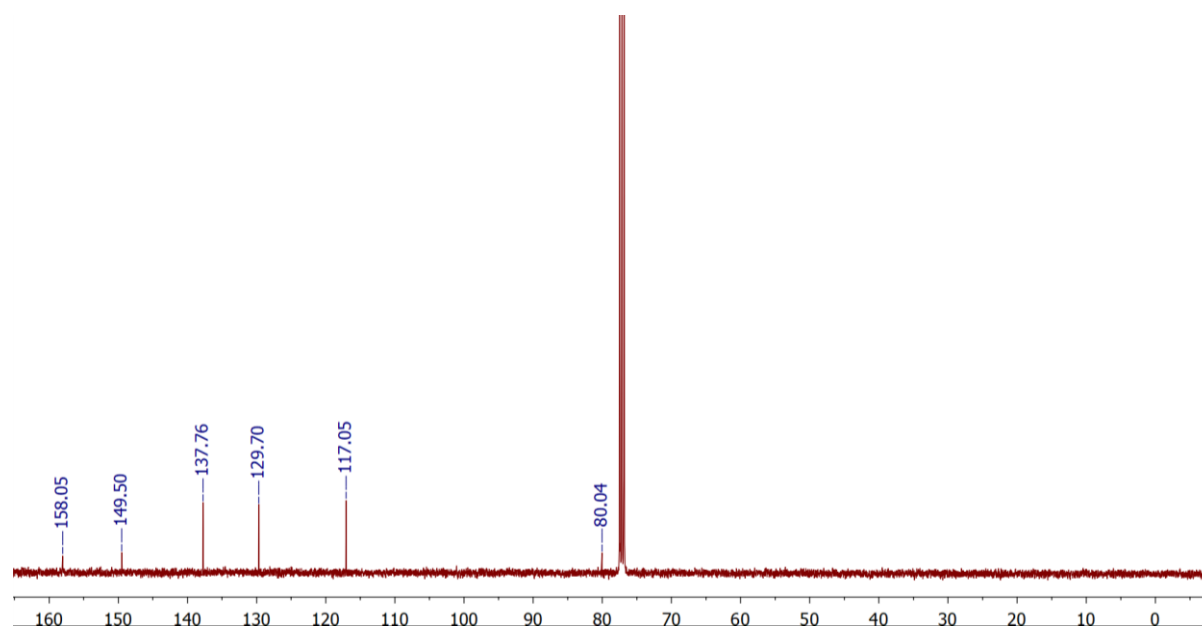
^{1}H NMR and ^{13}C NMR Spectra of 19

Figure S35: ^{1}H NMR Spectrum of **19** in CDCl$_3$ (δ CHCl$_3$ 7.26)
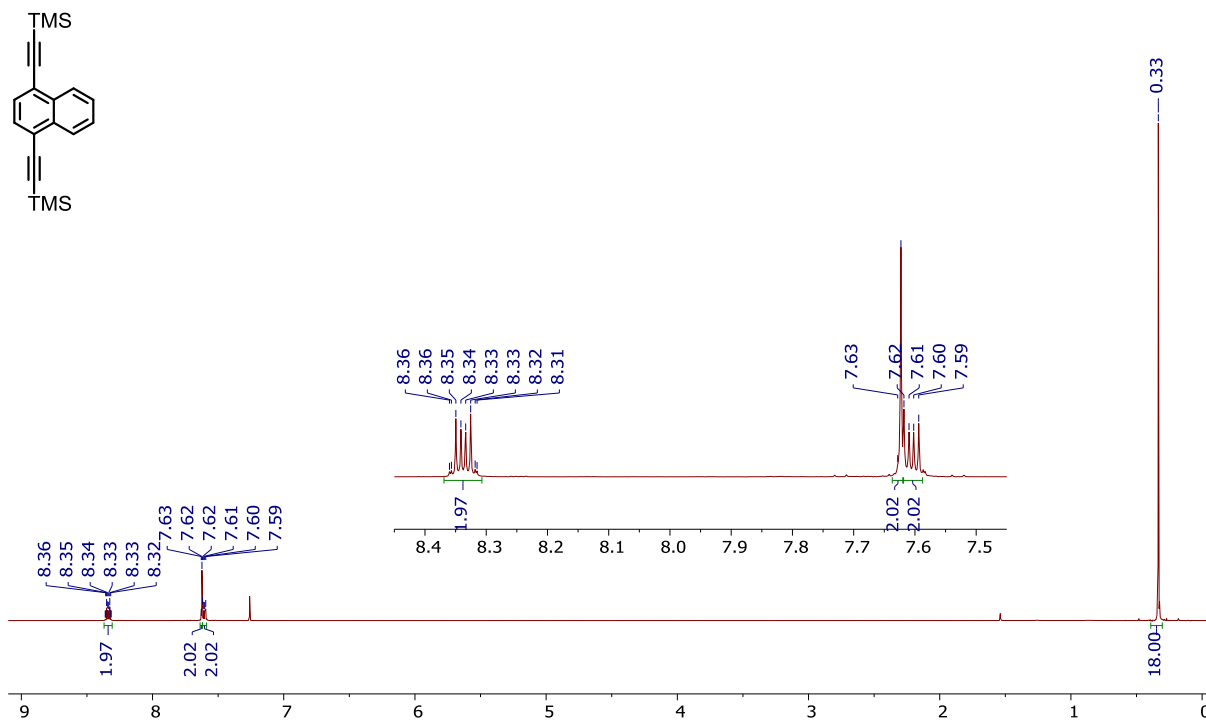
Figure S36: ^{13}C NMR Spectrum of **19** in CDCl$_3$ (δ 77.16)
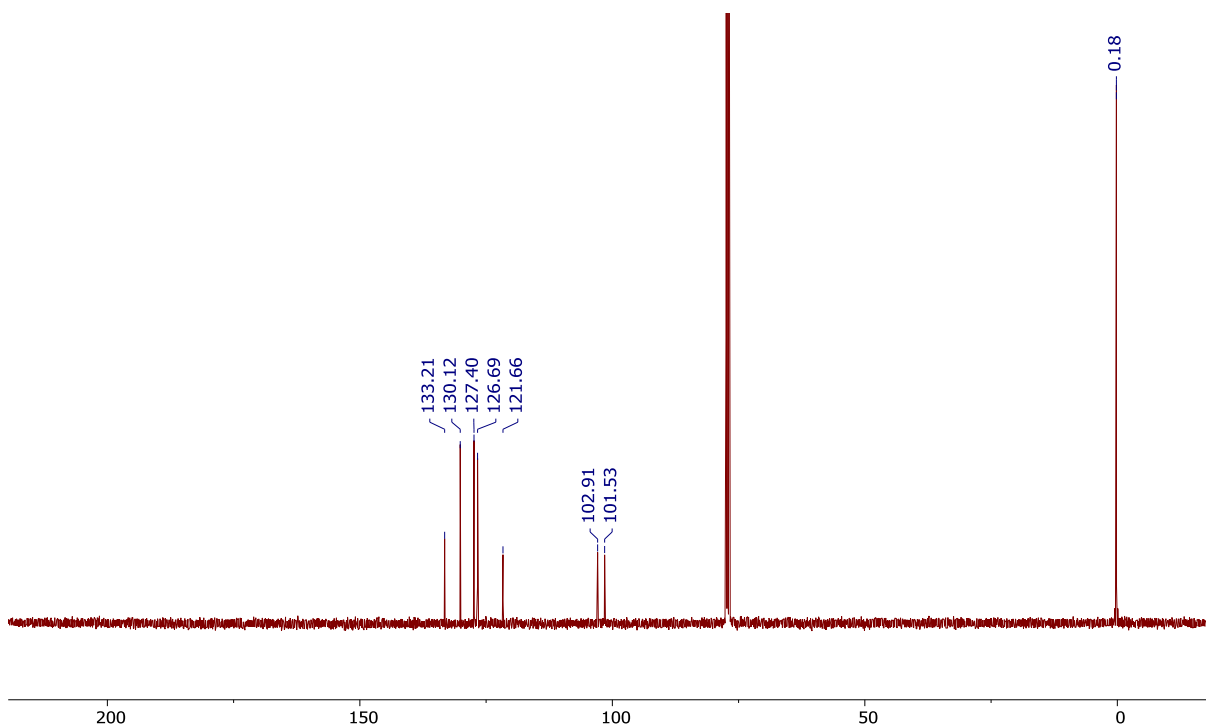
^{1}H NMR and ^{13}C NMR Spectra of 20

Figure S37: ^{1}H NMR Spectrum of **20** in CDCl$_3$ (δ CHCl$_3$ 7.26)
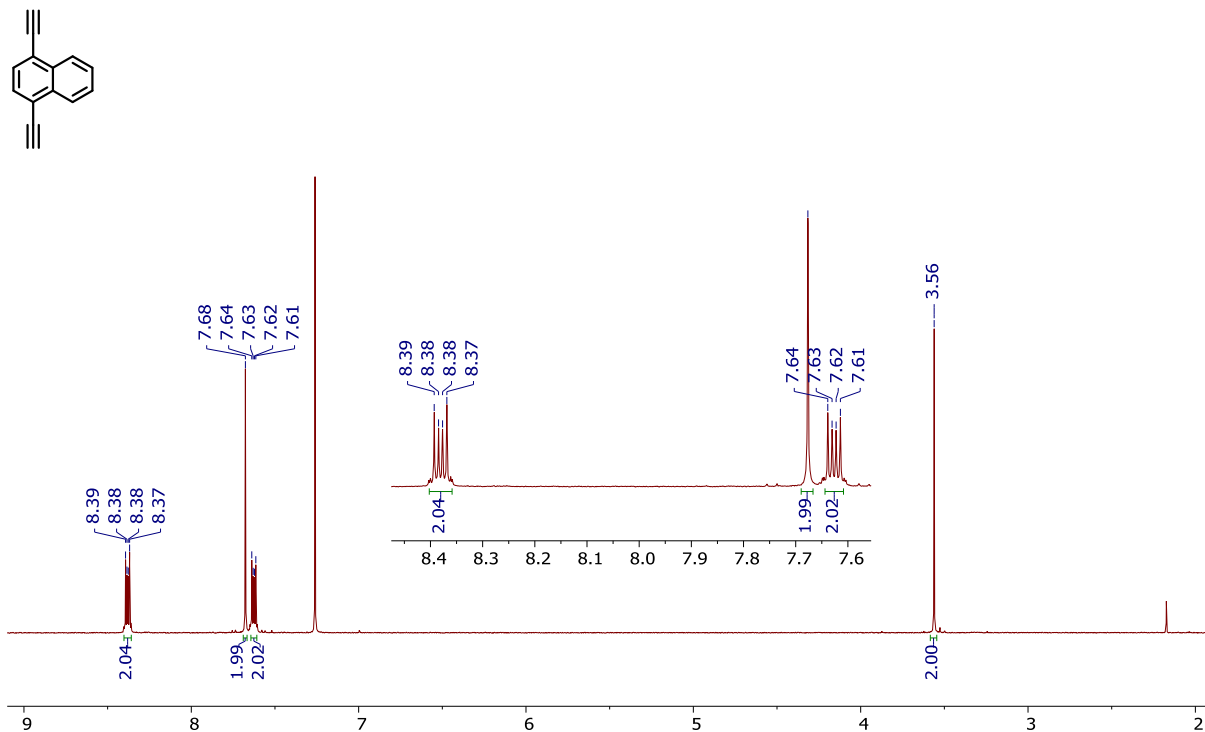
Figure S38: ^{13}C NMR Spectrum of **20** in CDCl$_3$ (δ 77.16)
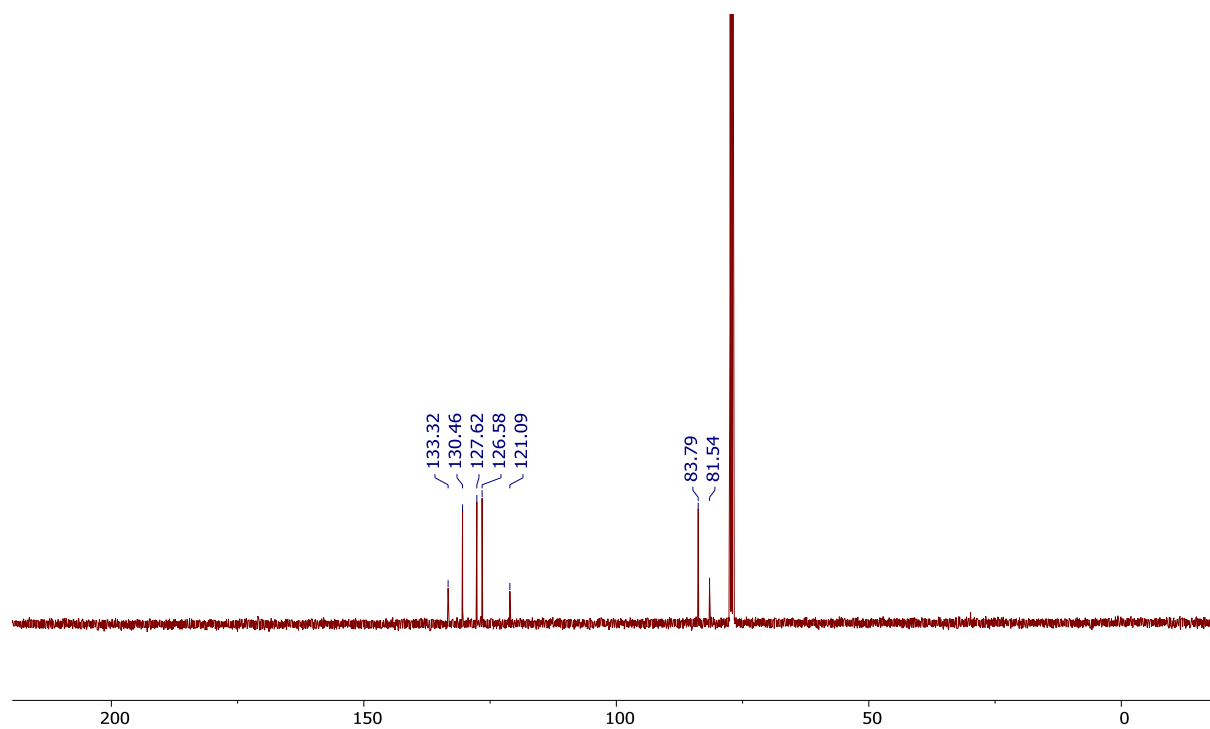
^{1}H NMR and ^{13}C NMR Spectra of 22

Figure S39: ^{1}H NMR Spectrum of **22** in CDCl$_3$ (δ CHCl$_3$ 7.26)
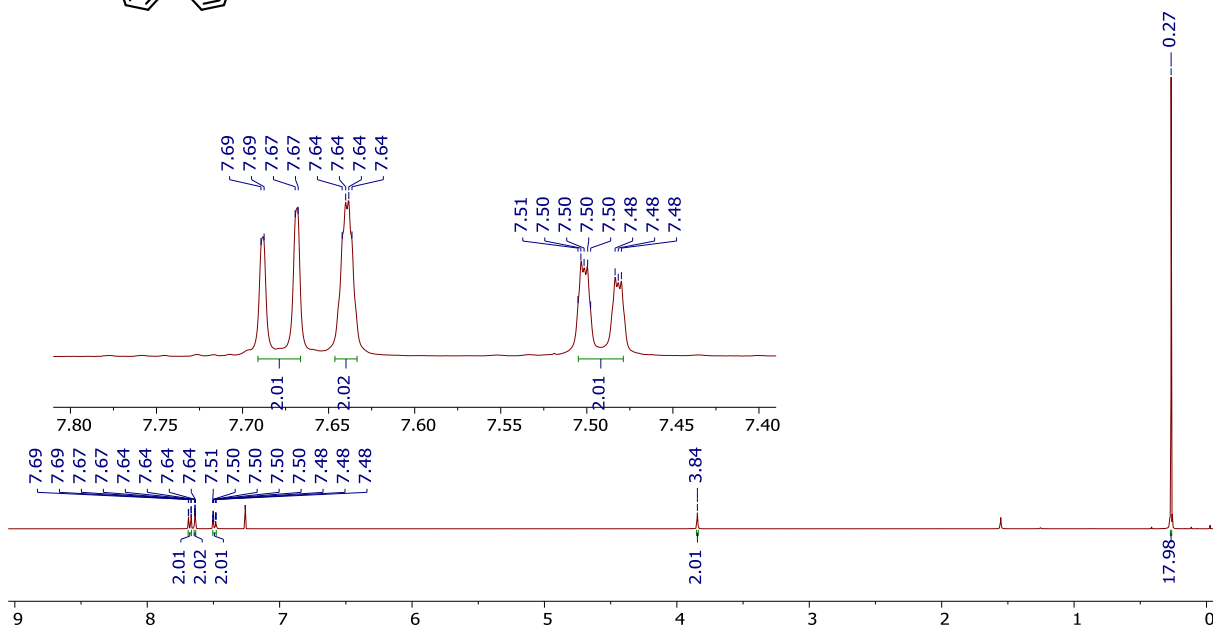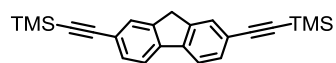
Figure S40: ^{13}C NMR Spectrum of **22** in CDCl$_3$ (δ 77.16)
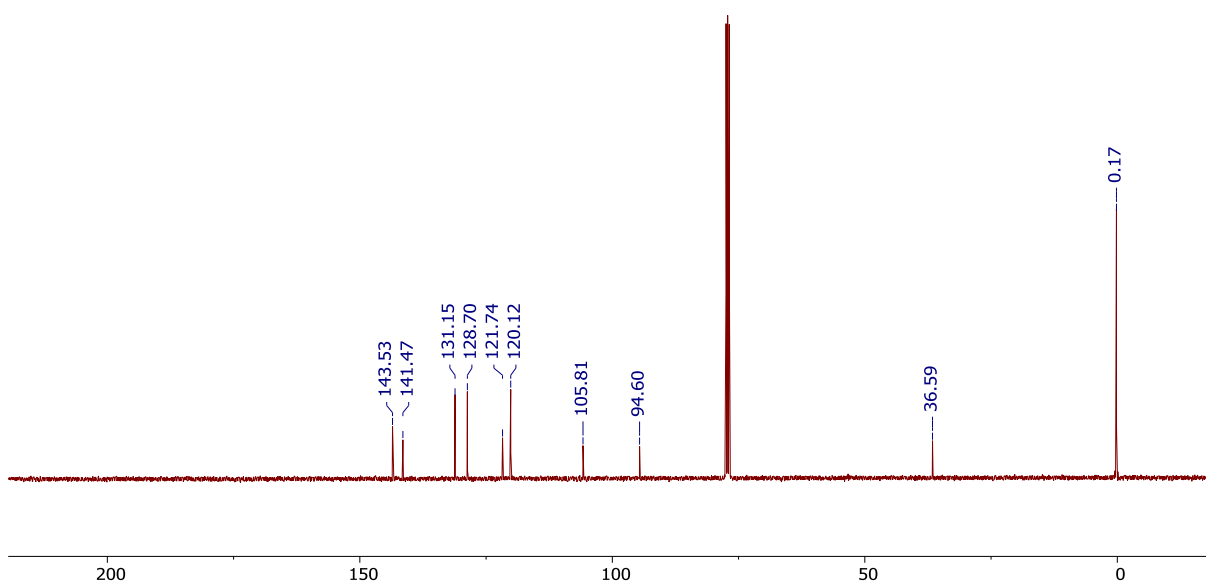
^{1}H NMR and ^{13}C NMR Spectra of 23

Figure S41: ^{1}H NMR Spectrum of **23** in CDCl$_3$ (δ CHCl$_3$ 7.26)
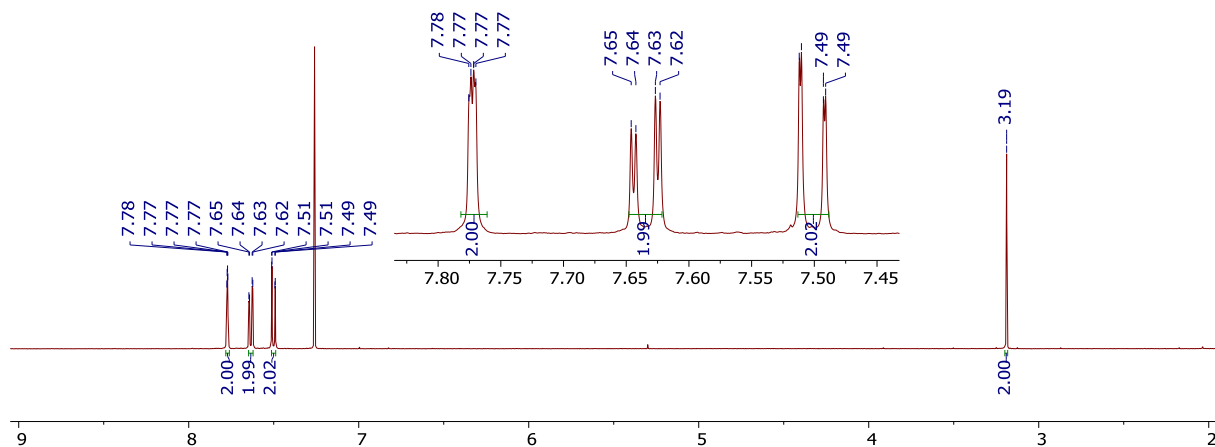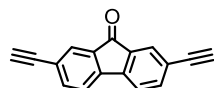
Figure S42: ^{13}C NMR Spectrum of **23** in CDCl$_3$ (δ 77.16)
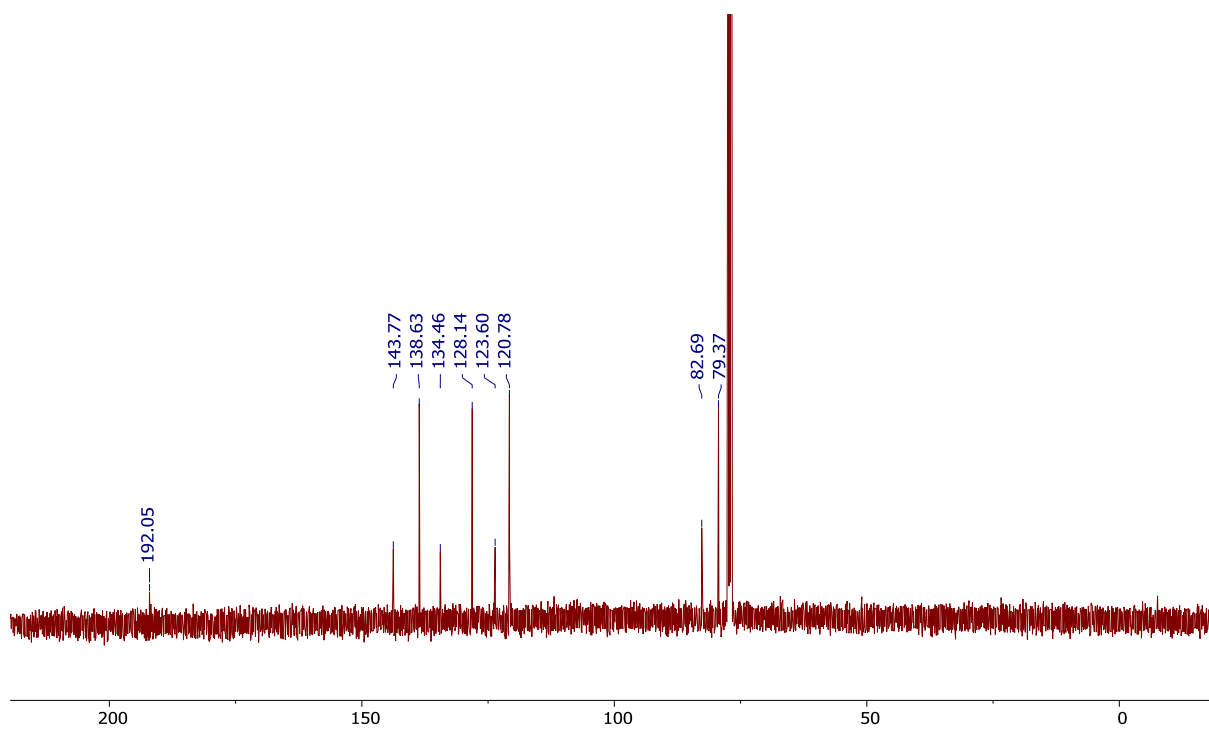
Figure S43: ^{1}H NMR Spectrum of **24** in CDCl$_3$ (δ CHCl$_3$ 7.26)
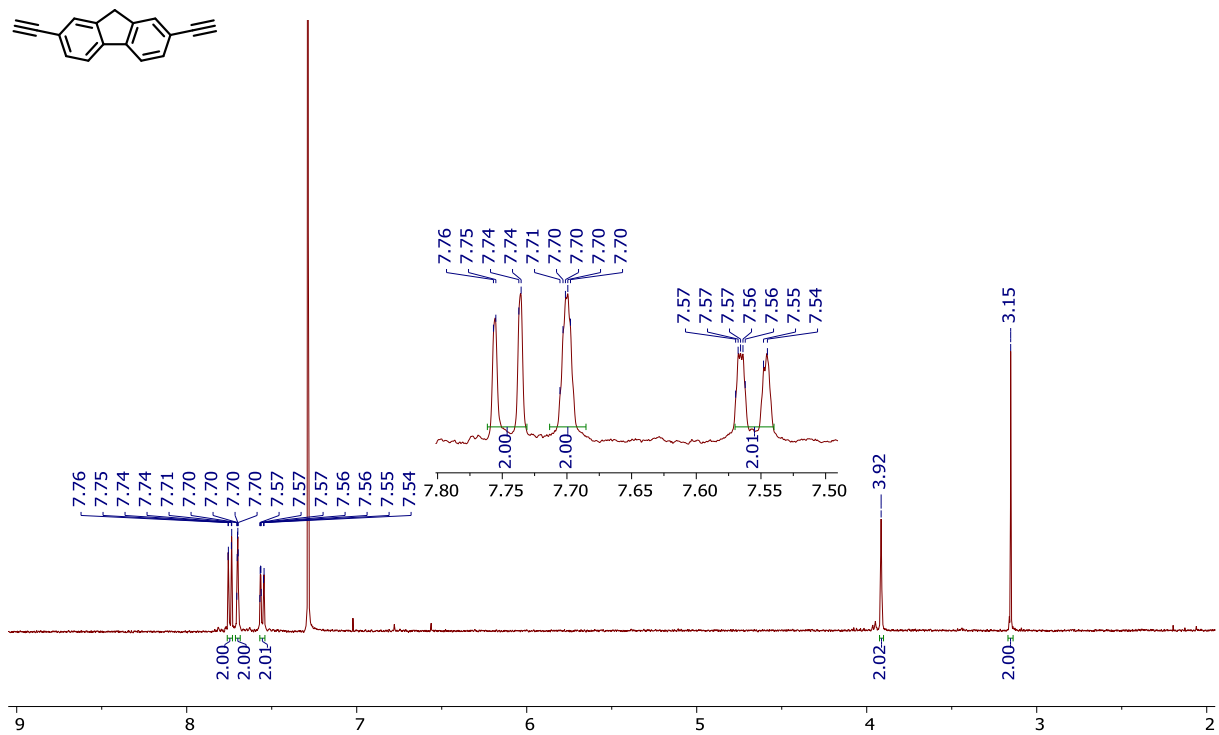
^{1}H NMR and ^{13}C NMR Spectra of 28

Figure S44: ^{1}H NMR Spectrum of **28** in CDCl$_3$ (δ CHCl$_3$ 7.26)
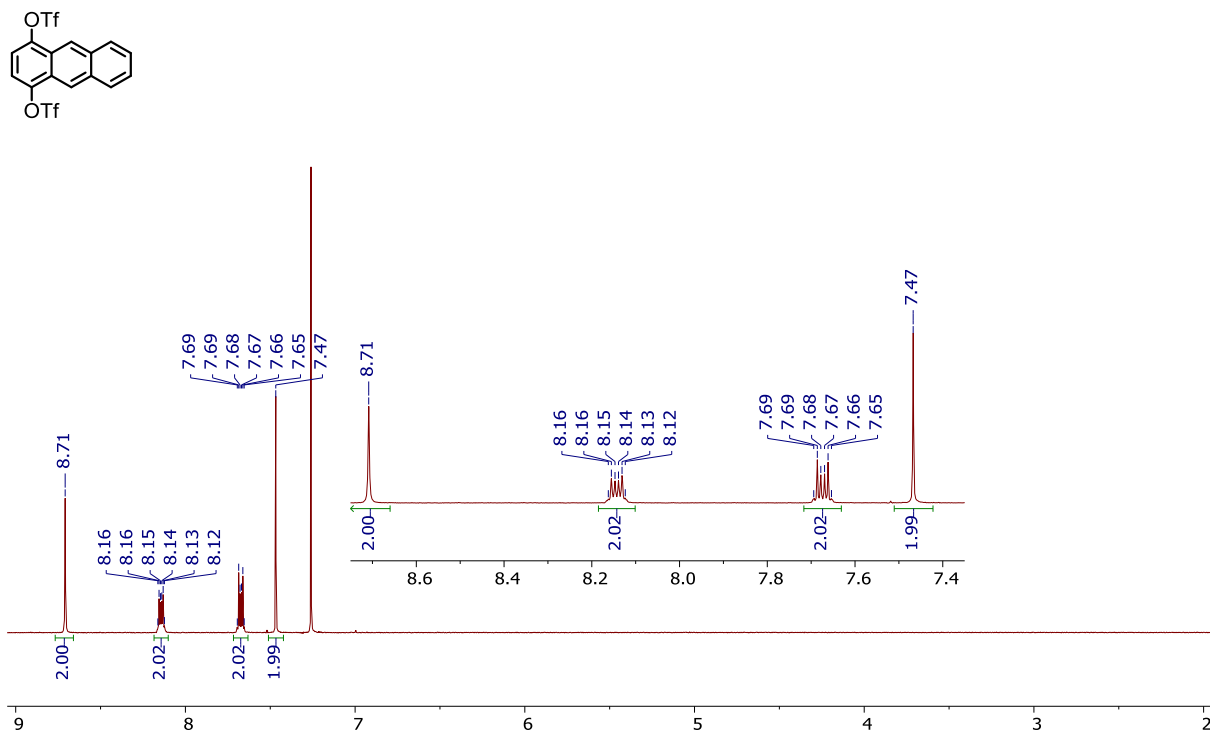
Figure S45: ^{13}C NMR Spectrum of **28** in CDCl$_3$ (δ 77.16)
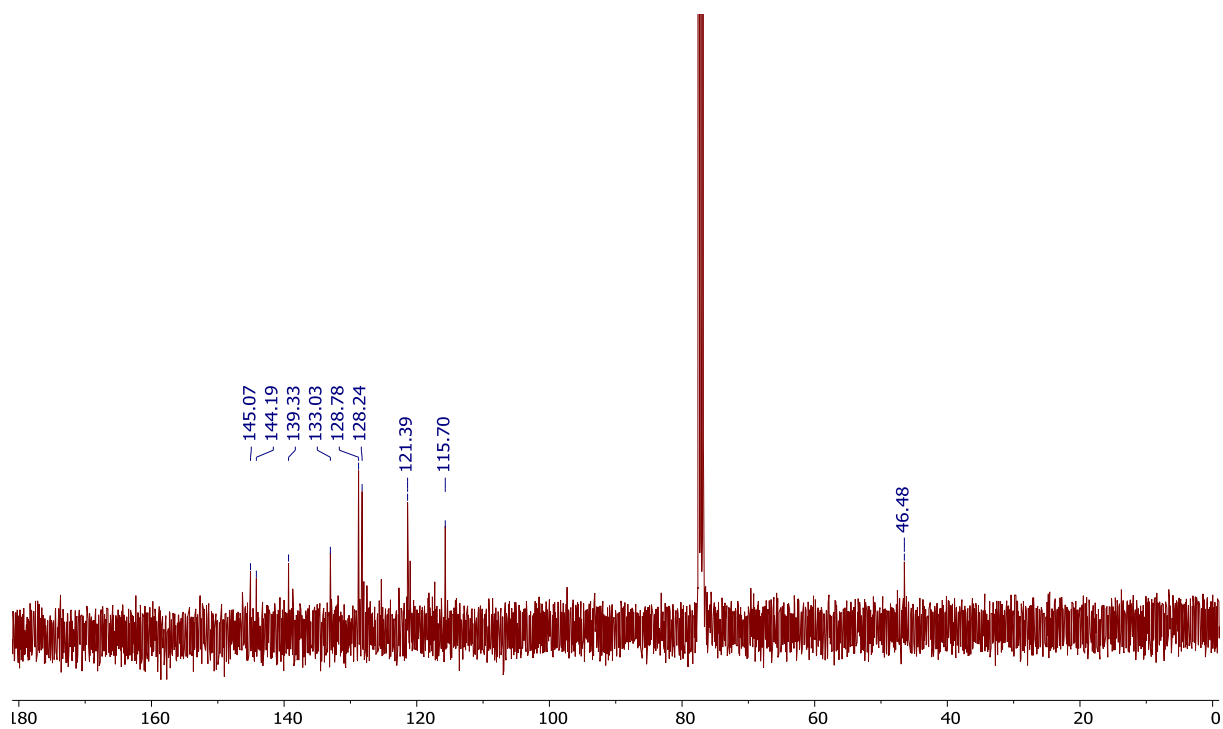
^{1}H NMR and ^{13}C NMR Spectra of 29

Figure S46: ^{1}H NMR Spectrum of **29** in CDCl$_3$ (δ CHCl$_3$ 7.26)
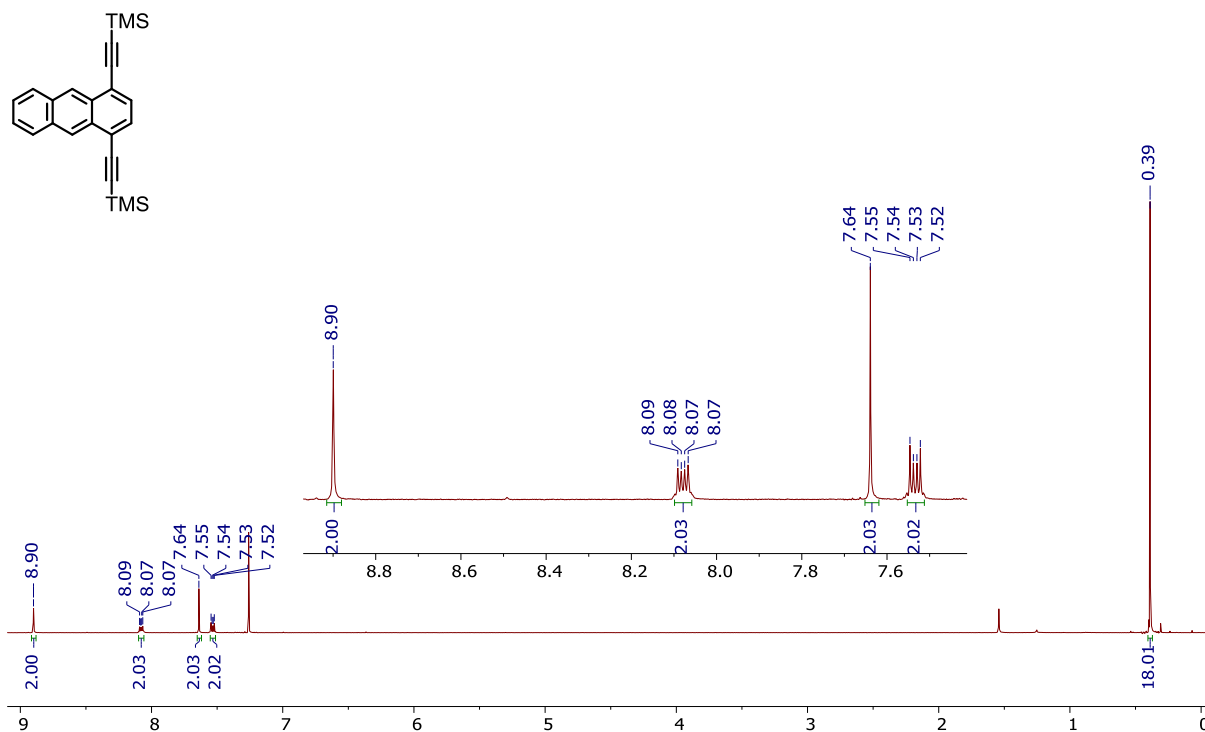
Figure S47: ^{13}C NMR Spectrum of **29** in CDCl$_3$ (δ 77.16)
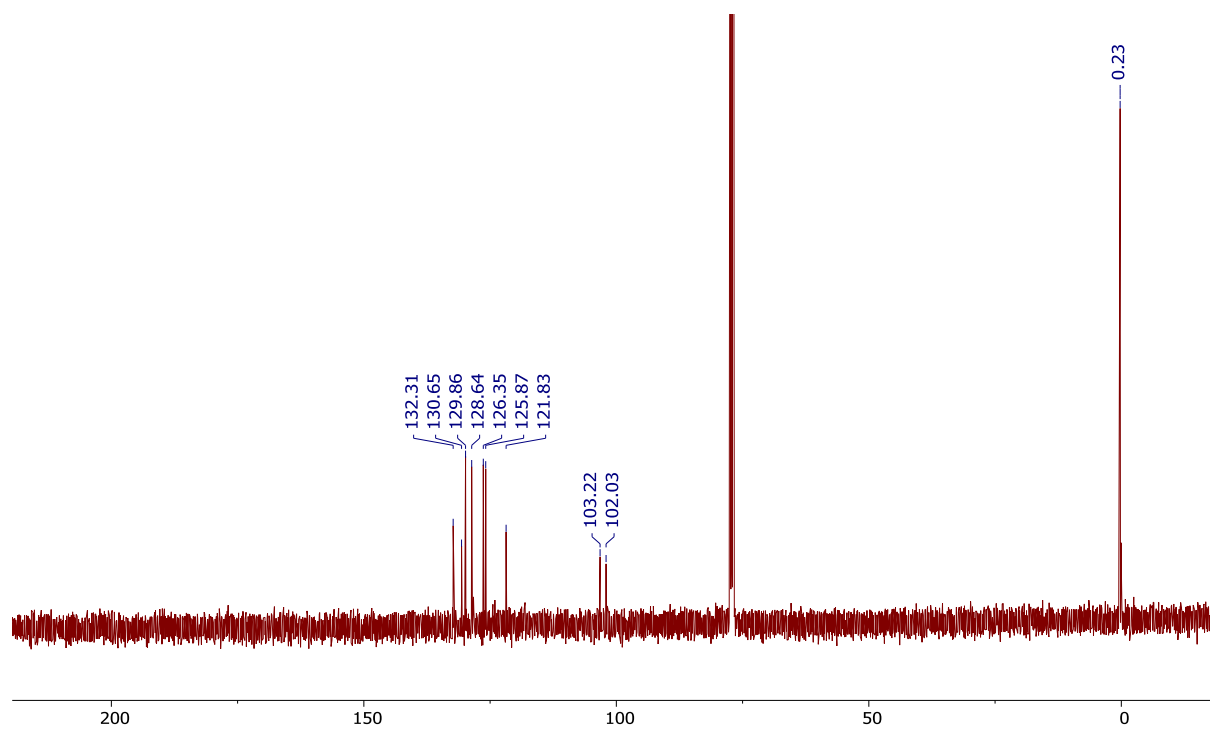
^{1}H NMR Spectra of 30

Figure S48: ^{1}H NMR Spectrum of **30** in CDCl$_3$ (δ CHCl$_3$ 7.26)
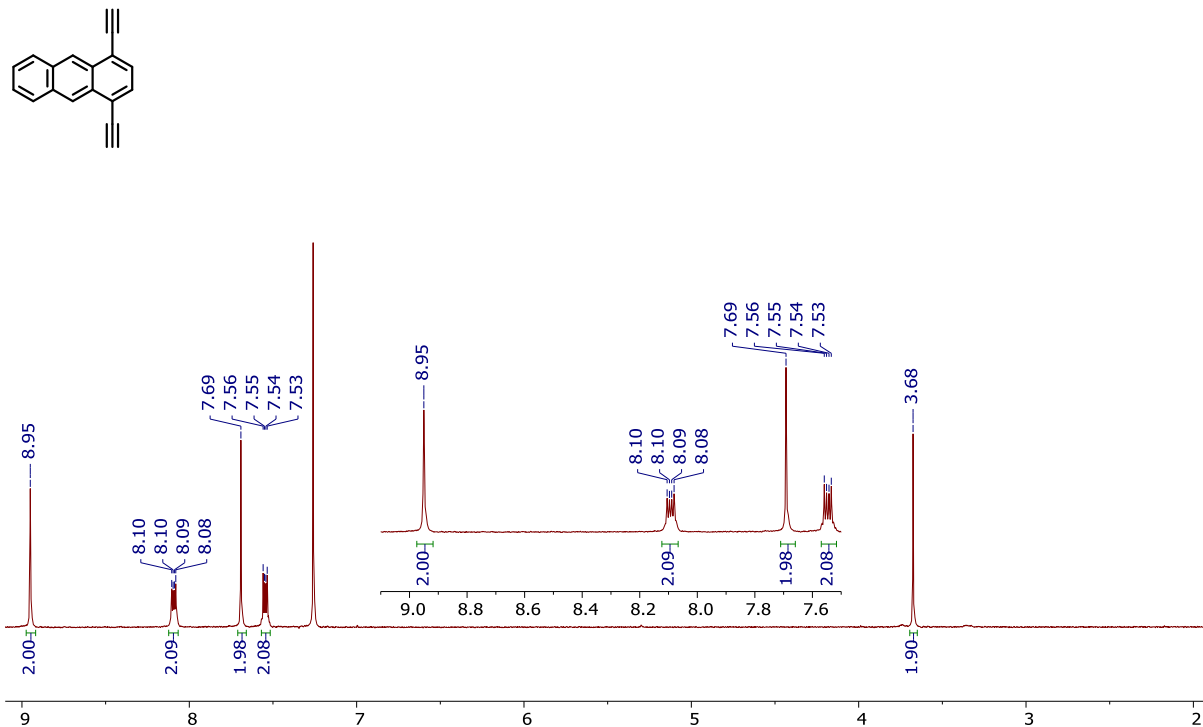
^{1}H NMR and ^{13}C NMR Spectra of 32

Figure S49: ^{1}H NMR Spectrum of **32** in CDCl$_3$ (δ CHCl$_3$ 7.26)
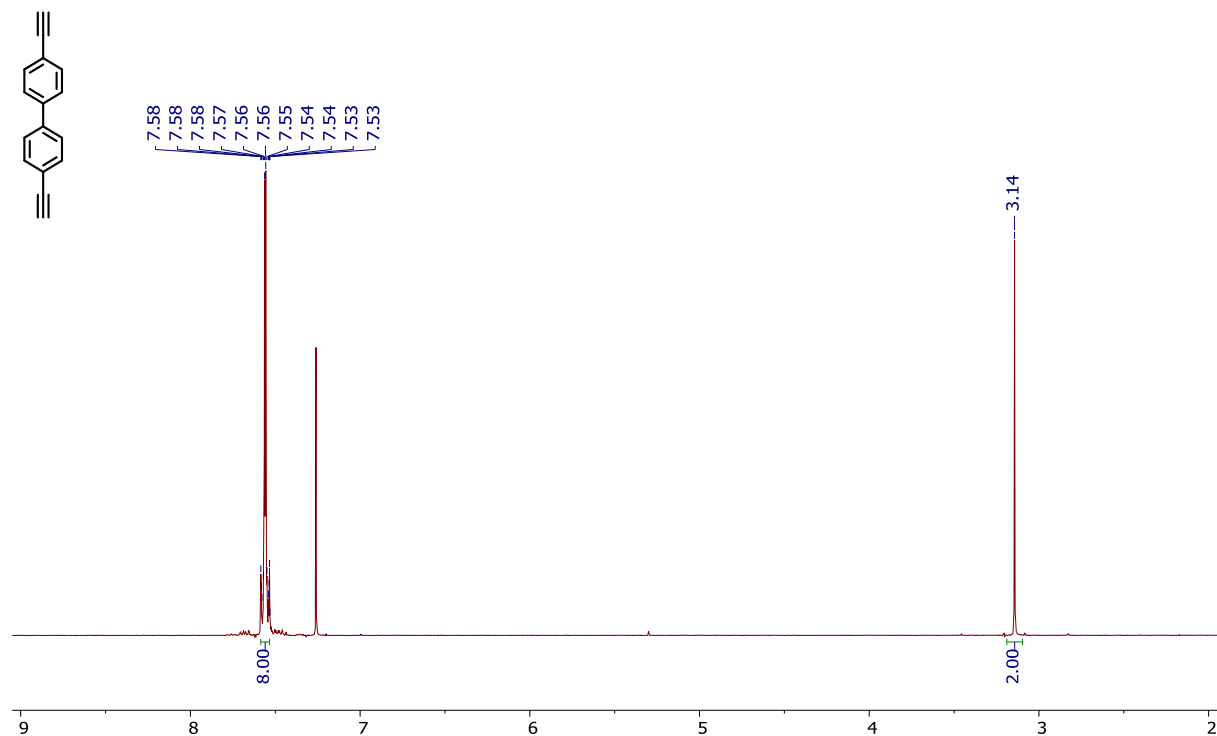
Figure S50: ^{13}C NMR Spectrum of **32** in CDCl$_3$ (δ 77.16)
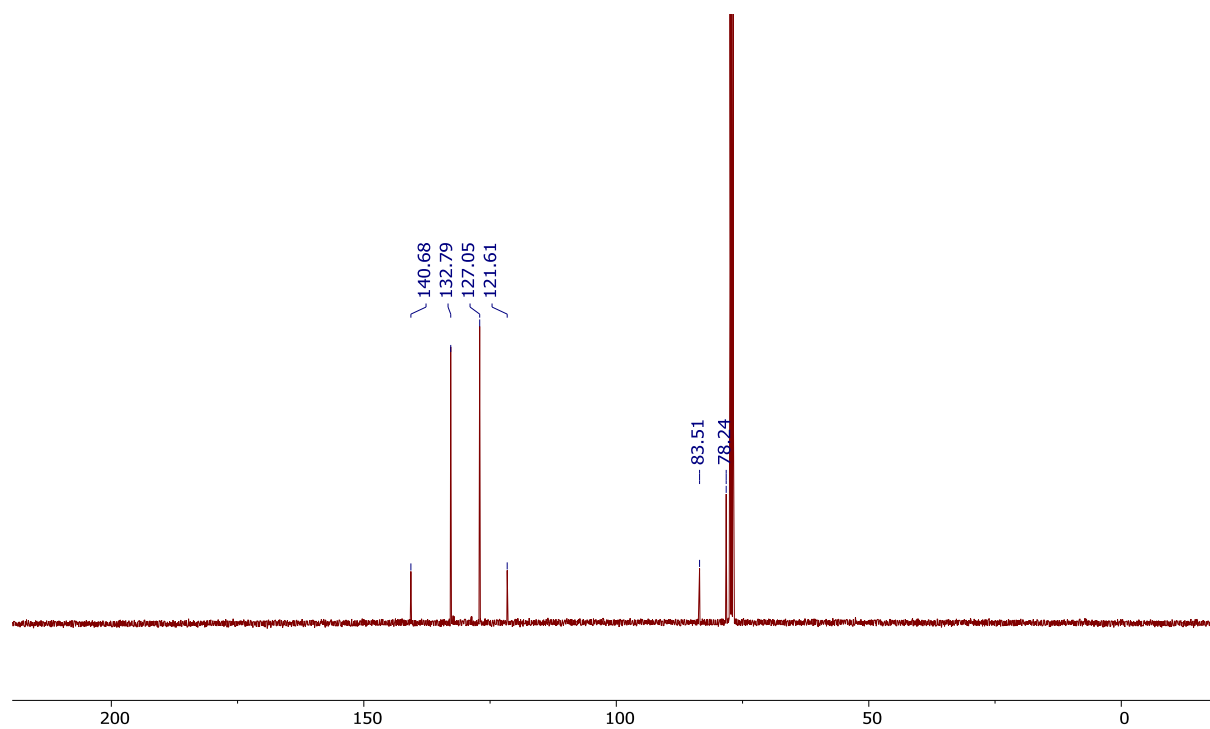
6. References for the Supporting Information

1   G. Meszaros, C. Li, I. Pobelov and T. Wandlowski, *Nanotechnology,* 2007, **18**, 424004.

2   Y. Yang, J.-Y. Liu, Z.-B. Chen, J.-H. Tian, X. Jin, B. Liu, X. Li, Z.-Z. Luo, M. Lu, F.-Z. Yang, N. Tao and Z.-Q. Tian, Conductance histogram evolution of an EC–MCBJ fabricated Au atomic point contact. *Nanotechnology,* 2011, **22**, 275313.

3   A. A. Deniz, K. S. Peters and G. J. Snyder, *Science,* 1999, **286**, 1119-1122.

4   T. C. W. Mak and J. Trotter, *J. Chem. Soc.* 1962, 1.

5   G. Fraenkel, Y. Asahi, M. Mitchell and M. Cava, *Tetrahedron,* 1964, **20**, 1179-1184.

6   (a) C. J. Lambert and S. X. Liu, *Chem. – Eur. J.,* 2018, **24**, 4193-4201; (b) T. Tada and K. Yoshizawa, *ChemPhysChem.*, 2002, **3**, 1035–1037.

7   J. M. Soler, E. Artacho, J. D. Gale, A. Garcia, J. Junquera, P. Ordejon and D. Sanchez-Portal, *J. Phys.: Condens. Matter,* 2002, **14**, 2745-2779.

8   J. Ferrer, C. J. Lambert, V. M. García-Suárez, D. Z. Manrique, D. Visontai, L. Oroszlany, R. Rodríguez-Ferradás, I. Grace, S. W. D. Bailey, K. Gillemot, *et. al. New J. Phys.,* 2014, **16**, 093029.

9   D. Lehnherr, J. M. Alzola, E. B. Lobkovsky and W. R. Dichtel, *Chem. – Eur. J.,* 2015, **21**, 18122–18127.

10 C. W. Keyworth, K. L. Chan, J. G. Labram, T. D. Anthopoulos, S. E. Watkins, M. McKiernan, A. J. P. White, A. B. Holmes and C. K. Williams, *J. Mater. Chem.,* 2011, **21**, 11800–11814.

11 D. H. Hua, M. Tamura, X. Huang, H. A. Stephany, B. A. Helfrich, E. M. Perchellet, B. J. Sperfslage, J.-P. Perchellet, S. Jiang, D. E. Kyle and P. K. Chiang, *J. Org. Chem.,* 2002, **67**, 2907–2912.